1. Report No. ABC-UTC-UW 2016-3-2 -Final	2. Government Accession No.	3. Recipient's Catalog No.	
4. Title and Subtitle **Economic Pier-to-Pile Connections for Permanently Cased Shaft (CFST) Piles**		5. Report Date September 9, 2022 6. Performing Organization Code	
7. Author(s) Dawn E. Lehman, Charles W. Roeder and Spencer Lindsley Orcid ID: 0000-0002-0823-1167		8. Performing Organization Report No.	
9. Performing Organization Name and Address Department of Civil and Environmental Engineering University of Washington 201 More Hall Seat, WA 98195-2700		10. Work Unit No. (TRAIS) 11. Contract or Grant No. Enter the correct number: 69A3551747121	
12. Sponsoring Organization Name and Address Accelerated Bridge Construction University Transportation Center Florida International University 10555 W. Flagler Street, EC 3680 Miami, FL 33174 US Department of Transportation Office of the Assistant Secretary for Research and Technology And Federal Highway Administration 1200 New Jersey Avenue, SE Washington, DC 201590		13. Type of Report and Period Covered Final Report Jan. 2020 to Jan. 2021 14. Sponsoring Agency Code	
15. Supplementary Notes			
16. Abstract This is an initial study into a direct connection between Reinforced Concrete (RC) piers and Concrete filled steel tubes (CFSTs) piles or drilled shafts for accelerated construction of high-speed rail and other transportation systems. CFSTs are composite structural components consisting of a steel tube with concrete infill. They have greater strength and stiffness than typical RCs structural elements of comparable size, and permit accelerated construction because no internal reinforcement, shoring or formwork is required. CFST is suitable for piles and drilled shafts, but there has been little research on connections of RC columns to CFST piles and drilled shafts. This research is an experimental study of a new direct connection between these members. In this research, half-scale column-to-pile connections were tested to evaluate their inelastic behavior under seismic loading. Two specimens were tested with the primary focus on the nonlinear behavior and effect of the relative size of the RC pier to the CFST pile. The transfer of the force and moment from the RC column to the CFST pile were closely monitored. The experiments showed that the connections have excellent strength, ductility, and inelastic deformation capacity. The moment and force of the RC column were effectively transferred to the CFST pile with a nominal development length of the reinforcing bar. The test suggests that connections with a larger pile provide slightly better seismic performance, but only preliminary recommendations can be made based upon this limited test program.			
17. Key Words Connections, Concrete Filled Tubes, Pier Columns, Piles		18. Distribution Statement No restrictions.	
19. Security Classification (of this report) Unclassified.	20. Security Classification (of this page) Unclassified.	21. No. of Pages 103	22. Price

Form DOT F 1700.7 (8-72) Reproduction of completed page authorized

(this page is intentionally left blank)

ECONOMIC PIER-TO-PILE CONNECTIONS FOR PERMANENTLY CASED SHAFT (CFST) PILES

Final Report
April 2022

Principal Investigator: Dawn E. Lehman and Charles W. Roeder
Department of Civil and Environmental Engineering
Florida International University

Authors
Spencer Lindsley, Dawn E. Lehman and Charles W. Roeder

Sponsored by
Accelerated Bridge Construction University Transportation Center

ACCELERATED BRIDGE CONSTRUCTION
UNIVERSITY TRANSPORTATION CENTER

A report from
Department of Civil and Environmental Engineering
University of Washington
More Hall, Box 352700
Seattle WA 98103
Phone: 206-715-2108
https://www.ce.washington.edu

DISCLAIMER

The contents of this report reflect the views of the authors, who are responsible for the facts and the accuracy of the information presented herein. This document is disseminated in the interest of information exchange. The report is funded, partially or entirely, by a grant from the U.S. Department of Transportation's University Transportation Program. However, the U.S. Government assumes no liability for the contents or use.

CONTENTS

DISCLAIMER ..... **IV**

CHAPTER 1. INTRODUCTION **1**

1.1 RESEARCH MOTIVATION **1**
1.2 RESEARCH OBJECTIVES **2**
1.3 ORGANIZATION OF REPORT **2**

CHAPTER 2. LITERATURE REVIEW **4**

2.1 CONNECTION TYPES AND CODE PROVISIONS **4**
2.2 TEST PROGRAMS **9**
2.2.1 LATERAL BEHAVIOR OF RC COLUMNS SUPPORTED ON TYPE II SHAFTS: LIU (2012) 9
2.2.2 SEISMIC PERFORMANCE OF BRIDGE COLUMN-PILE-SHAFT PIN CONNECTIONS FOR APPLICATIONS IN ACCELERATED BRIDGE CONSTRUCTION: MEHRAEIN (2016) 14
2.2.3 SEISMIC PERFORMANCE OF COLUMN TO DRILLED SHAFTS: CHANG (2021) 20
2.3 CFST CONNECTIONS **24**
2.3.1 PERFORMANCE OF STEEL PIPE PILE-TO-CONCRETE CAP CONNECTIONS SUBJECTED TO SEISMIC OR HIGH TRANSVERSE LOADING: KAPPES (2013) 24
2.3.2 DESIGN EXPRESSIONS AND DYNAMIC EVALUATION OF CFST BRIDGES SUBJECTED TO SEISMIC HAZARDS: STEPHENS (2016) 27

CHAPTER 3. EXPERIMENTAL TEST PROGRAM **32**

3.1 DESIGN AND CONSTRUCTION OF TEST SPECIMENS **32**
3.2 SPECIMEN MATERIALS **37**
3.2.1 CONCRETE 37
3.3 EXPERIMENTAL TEST SETUP **41**
3.4 INSTRUMENTATION **44**
3.5 TEST PROTOCOL **47**

CHAPTER 4. EXPERIMENTAL OBSERVATIONS AND RESULTS **49**

4.1 INTRODUCTION **49**

4.2 SPECIMEN 30-21 49
4.2.1 LOW DRIFT CYCLES (0-2.0% DRIFT) 53
4.2.2 MODERATE DRIFT CYCLES (2.0-4.0% DRIFT) 56
4.2.3 LARGE DRIFT CYCLES (GREATER THAN 4.0% DRIFT) 59
4.3 SPECIMEN 48-21 65
4.3.1 LOW DRIFT CYCLES (0-2.0% DRIFT) 69
4.3.2 MODERATE DRIFT CYCLES (2.0-4.0% DRIFT) 75
4.3.3 LARGE DRIFT CYCLES (GREATER THAN 4.0% DRIFT) 76

CHAPTER 5. SUMMARY AND CONCLUSIONS 82

5.1 SUMMARY OF RESEARCH 82
5.2 RESEARCH RESULTS AND CONCLUSIONS 83

LIST OF FIGURES

Figure 2.1. General Pin Connection 5
Figure 2.2. Column-Shaft Connection Types (Caltrans) 6
Figure 2.3. CFST-to Column Connection (WSDOT BDM) 9
Figure 2.4. Liu (2012) Column Reinforcement Cages: a) Specimen 1 and b) Specimen 2 10
Figure 2.5. Liu (2012) Shaft Reinforcement Cages: a) Specimen 1 and b) Specimen 2 11
Figure 2.6. Liu (2012) Test Setup: a) Specimen 1 and b) Specimen 2 12
Figure 2.7. Liu (2012) Buckling and Fracture of Longitudinal Bars: a) Specimen 1 and b) Specimen 2 13
Figure 2.8. Liu (2012) Overall Responses of Column-Shaft Assemblies including P-Δ Effects a) Test 1 and b) Test 2 13
Figure 2.9. Mehraein (2016) BPSA Pipe-Pin Detail 15
Figure 2.10. Mehraein (2016) BRSA Rebar Hinge Detail 15
Figure 2.11. Mehraein (2016) BPSA Elevation View 16
Figure 2.12. Mehraein (2016) BRSA Elevation View 16
Figure 2.13. Mehraein (2016) Shake Table Setup 17
Figure 2.14. Mehraein (2016) Force-Displacement Curve a) BPSA CIP and b) BPSA PC 18
Figure 2.15. Mehraein (2016) BPSA Connection After Final Run a) CIP and b) PC 18
Figure 2.16. Mehraein (2016) Force-Displacement Curve a) BRSA CIP and b) BPSA PC 19
Figure 2.17. Mehraein (2016) BRSA Connection After Final Run a) CIP and b) PC 19
Figure 2.18. Chang (2021) Test Setup 21
Figure 2.19. Chang (2021) Moment-Drift Response of DS-4 21
Figure 2.20. Final State of Specimens a) DS-1, b) DS-2, c) DS-3, and d) DS-4 22
Figure 2.21. CFST to Pier Cap Connection (Kappes 2013) 24
Figure 2.22. General Test Setup Layout (all lengths in units of in.) (Kappes 2013) . 26
Figure 2.23. Final State of Specimens a)VT1 b) CT2 (Kappes 2013) 26

Figure 2.24. Moment-Drift of Specimen CT2 (Kappes 2013) 27
Figure 2.25. CFST to Pier Cap Connections (Stephens 2016) 28
Figure 2.26. Moment-Drift Behavior of ER Connection (Stephens 2016) 29
Figure 2.27. Moment-Drift Behavior of WD Connection (Stephens 2016) 29
Figure 2.28. Moment-Drift Behavior of RC Connection (Stephens 2016) 30
Figure 3.1. Specimen Layout and Dimensions a) Cross-section view b) Plan view .. 33
Figure 3.2. Transfer Block Reinforcement a) Specimen 30-21 and b) Specimen 48-21 35
Figure 3.3. Specimen 30-21 Reinforcement 36
Figure 3.4. Specimen Reinforcement a) Specimen Elevation and Reinforcement and b) Specimen 48-21 Completed Reinforcement Cage 36
Figure 3.5. Tested Concrete Cylinders in a) Compression, b) Tension, and c) Elastic Modulus 38
Figure 3.6. Reinforcement Tensile Test Setup 40
Figure 3.7. a) 48 in. and b) 30 in. Diameter Steel Tubes Cut to Size 40
Figure 3.8. Annular Rings for Specimens 30-21 and 48-21 41
Figure 3.9. Experimental Setup Overview 42
Figure 3.10. Axial Bearing Assembly for Specimen 30-21 43
Figure 3.11. Axial Bearing Assembly 44
Figure 3.12. General Instrumentation Layout 45
Figure 3.13. Target Displacement History 48
Figure 1.1. Specimen 30-21 Force-Displacement Curve 49
Figure 1.2. Specimen 30-21 Moment-Drift Curve with P-Δ Effects Removed 50
Figure 1.3. Specimen 30-21 Normalized by F_n Force-Drift Curve with P-Δ Effects Removed 50
Figure 1.4. Specimen 30-21 Normalized by M_n Moment-Drift Curve with P-Δ Effects Removed 51
Figure 1.5. Specimen 30-21 Horizontal Cracks on North Column Face 52
Figure 1.6. Specimen 30-21 Strain Distribution at 1.1% Drift 53
Figure 1.7. Specimen 30-21 Interface Cracks on Southern Face at 0.9% Drift 54

Figure 1.8. Specimen 30-21 Radial Cracks on North Face of Column 54

Figure 1.9. Specimen 30-21 Strain Distribution at 1.5% Drift 55

Figure 1.10. Specimen 30-21 Initial Spalled Region on North Face at 2.2% Drift 56

Figure 1.11. Specimen 30-21 Strain Distribution at 2.2% drift 56

Figure 1.12. Specimen 30-21 Spalled Region on Northern Column Face at 3.7% Drift 57

Figure 1.13. Specimen 30-21 Strain Distribution at 3.7% drift 58

Figure 1.14. Specimen 30-21 Exposed Longitudinal Reinforcement on South Face 58

Figure 1.15. Specimen 30-21 Strain Distribution at 5% Drift 59

Figure 1.16. Specimen 30-21 Original Moment-Drift Curve 60

Figure 1.17. Specimen 30-21 Corrected Moment-Drift Curve 60

Figure 1.18. Specimen 30-21 a) Major Spalled Region on Southern Column Face, b) Large Crack at Northern Column Interface at 7.3 % Drift 61

Figure 1.19. Specimen 30-21: Failed Specimen 30-21 at 8% Drift 62

Figure 1.20. Top of Specimen 30-21 Pile with Column Removed 63

Figure 1.21. Specimen 48-21 Force-Displacement Curve 65

Figure 1.22. Specimen 48-21 Moment-Drift Curve with P-Δ Effects Removed 66

Figure 1.23. Specimen 48-21 Force-Displacement Curve with P-Δ Effects Removed Normalized by F_n 66

Figure 1.24. Specimen 48-21 Moment-Drift Curve with P-Δ Effects Removed Normalized by M_n 67

Figure 1.25. Specimen 48-21 Horizontal Cracks on North Column Face at 0.2% Drift 68

Figure 1.26. Specimen 48-21 Radial Cracks on Top of Pile Concrete at 0.8% Drift 69

Figure 1.27. Specimen 48-21 Strain Distribution at 0.8% Drift 70

Figure 1.28. Specimen 48-21 Vertical Residual Force Crack at 1.1% Drift 70

Figure 1.29. Specimen 48-21 Strain Distribution at 1.1% Drift 71

Figure 1.30. Specimen 48-21 Column Interface crack at 1.8% Drift 71

Figure 1.31. Specimen 48-21 Strain Distribution at 1.8% Drift 72

Figure 1.32. Specimen 48-21 Spalled Region at Base of North Face of Column at 2.6% Drift 72

Figure 1.33. Specimen 48-21 Strain Distribution at 2.6% Drift 73

Figure 1.34. Specimen 48-21 Exposed Transverse and Longitudinal Reinforcement at 4.1% Drift 74

Figure 1.35. Specimen 48-21 Strain Distribution at 4.1% Drift 75

Figure 1.36. Specimen 48-21 Buckled Longitudinal Reinforcement at 5.8% Drift 76

Figure 1.17. Specimen 48-21 North Face Severely Buckled Longitudinal Reinforcement Bars at 8.6% Drift 77

Figure 1.38. Final State of Specimen 48-21 after 9.7% drift 78

Figure 1.39. Top of Specimen 48-21 Pile with Column Removed 79

LIST OF TABLES

Table 2.1. Research Programs Reviewed 4
Table 2.2. Minimum Volumetric Ratio of Transverse Reinforcement in Caltrans Type II Shafts (Caltrans SDC) 7
Table 2.3. LIU (2012) Test Program 10
Table 2.4. Displacement Ductility of the column-shaft assemblies (Liu 2012) 14
Table 2.5. Mehraein (2016) Specifications of the Specimens 17
Table 2.6. Chang (2021) Test Program 20
Table 2.7. Kappes (2013) Test Program 25
Table 2.8. Kappes (2013) Summary of Test Results 26
Table 3.1. Specimen Test Matrix 32
Table 3.2. Material List 37
Table 3.3. Day of Test Concrete Properties 38
Table 3.4. Longitudinal Reinforcement Material Properties 39
Table 4.2. Maximum Resistances and Drifts in Each Cycle (30-21) 50
Table 4.3. Maximum Measured Crack Widths and Locations for Each Drift Level (30-21) 53
Table 4.4. Maximum Resistances and Drifts in Each Cycle (48-21) 66
Table 4.5. Maximum Measured Crack Widths and Locations for Each Drift Level (48-21) 69

ACKNOWLEDGEMENTS

This project was supported by the Accelerated Bridge Construction University Transportation Center (ABC-UTC at www.abc-utc.fiu.edu) at Florida International University (FIU), as lead institution, and Iowa State University (ISU) and the University of Nevada-Reno (UNR) as partner institutions. The authors would like to acknowledge the ABC-UTC support.
The author would like to extend special appreciation to the ABC-UTC and the U.S. Department of Transportation Office of the Assistant Secretary for Research and Technology for funding this project.

The author would like to thank all the State DOTs that participated in the survey; this work would not have been possible without their participation.
The author would like to thank the Research Advisory Panel members: Ahmad Abu-Hawash (Iowa DOT), James Corney (Utah DOT), Romeo Garcia (FHWA), and Bruce Johnson (Oregon DOT).

The authors also acknowledge additional funding provided by the Pacific Earthquake Engineering Research Center, and thank Amy Leland and Geoff Sweat of the Washington Department of Transportation for their advice and guidance. The assistance of the UW Laboratory Technician, Vongsant (Vince) Chaijaroen, in completing the research work is also gratefully acknowledged.

Chapter 1. INTRODUCTION

1.1 RESEARCH MOTIVATION

Concrete filled steel tubes (CFSTs) are a composite structural element that combines the compressive strength of concrete with the tensile strength and ductility of steel. They have been shown to provide greater strength and stiffness than traditional reinforced concrete (RC) elements of comparable size. CFSTs have significantly larger shear resistance than RC members of comparable size, and therefore CFSTs are very suitable for piles and drilled shafts in deep foundations at sites with liquefaction or lateral spreading of soil. CFSTs do not require formwork, shoring, or internal reinforcement, which accelerates construction and reduces cost.

In recent years, the seismic design forces on bridges have increased, which has led to increased demand on the structural resistance of bridge substructures. The use of CFSTs piles with RC columns provides the bridge with strength, stiffness, ductility, and energy dissipation for large lateral loads and deformations on the column and the pile. This combination also leads to accelerated construction and cost savings. However, connections between RC columns and CFST piles and the mechanism of force and moment transfer between the two components are not well understood. This research is an initial study investigating a direct connection between RC piers and CFST piles or drilled shafts for accelerated construction of high-speed rail or other transportation systems. The study focused on understanding these connections, their transfer mechanisms, and how these mechanisms affect moment, axial, and shear forces on the connection behavior.

Prior analytical research, suggests that the bond between the RC column reinforcement and the concrete, and the bond between the tube and concrete are important elements of the transfer

mechanism. The bond between the reinforcement and the concrete is dependent on the embedment depth of the reinforcement into the pile and the relative diameters of the column and pile. The bond between the tube and the concrete is affected by the type of steel tube used, with spirally welded tubes having shown to have more bond stress capacity than straight seam welded tubes. Adequate development length may be required to transfer the forces and moments of the RC column to the CFST pile.

This research is an experimental study to investigate a direct RC-column-to-CFST-pile connection. Two half-scale experiments are performed. The specimens are designed to consider the critical parameters noted above. The specimens are loaded under cyclic inelastic deformation and their inelastic behavior is measured and observed. The data is analyzed and the results are compared to determine the relative importance of the variables considered in the study.

1.2 Research Objectives

The experimental investigation examined the behavior of a direct CFST pile to RC column connection under cyclic loading and to provide initial design recommendations. In particular, the study investigates the inelastic behavior response of the reinforcement development length in a direct CFST pile-to-column connection and evaluates the effect of different pile diameters on the CFST pile-to-column connection behavior.

1.3 Organization of Report

This chapter is an introduction to the report. Chapter 2, is a literature review, which provides an overview of previous research that has been conducted on connections between cased shafts or concrete-filled tubes and RC columns, and other related work to this experimental research. Chapter 3, provides an overview of the two specimens in the test program and the testing apparatus and

instrumentation. Chapter 4, describes the experimental measured and observed response of the four tests, looking at the strain in the reinforcement, the specimen damage, and overall specimen behavior. Chapter 5 summarizes the work and the conclusions.

Chapter 2. LITERATURE REVIEW

This chapter contains an overview of current column-to-pile connections used in high seismic regions along with code requirements used by the Washington Department of Transportation (WSDOT) and the California Department of Transportation (Caltrans). Following this overview, are the experimental test programs that investigated the force-transfer mechanisms of these types of connections. Table 2.1 summarizes the different research programs and their focus.

Table 2.1. Research Programs Reviewed

Title	Researcher	Year	Research Focus
Lateral Behavior of RC Columns Supported on Type II Shafts	Liu	2012	Column Ductility and Plastic Hinge Formation
Performance of Steel Pipe Pile-to-Concrete Cap Connections Subjected to Seismic or High Transverse Loading	Kappes	2013	CFST Column to RC Cap Beam Connections
Design Expressions and Dynamic Evaluation of CFST Bridges Subjected to Seismic Hazards	Stephens	2016	CFST Column to Precast Cap Beam Connections
Seismic Performance of Bridge Column-Pile-Shaft Pin Connections for Applications in Accelerated Bridge Construction	Mehraein	2016	Pipe-Pin and Rebar-Pin Connections on RC Column to Shaft Connection
Analytical Investigation of A New Direct Column-to-Cased Shaft Connection	Zhao	2020	CFST Pile to RC Column Connections
Seismic Performance of Column-to-Drilled Shaft Connections in RC Bridges	Chang	2021	RC Drilled Shaft to CIP Column Connections

2.1 CONNECTION TYPES AND CODE PROVISIONS

Two general types of column-shaft connections are used in high seismic regions by Caltrans and WSDOT: pin connections transfer axial and shear force while permitting rotation, and restrained connections that transfer moment, axial, and shear forces while restraining rotation.

Pin connections between column-shaft assemblies typically having a reinforcement cage, pipe, or solid steel section as the pinned connection between the top of the shaft and the column base as shown in Figure 2.1. The main code requirements for this type of connection is that a) the shafts are designed to be capacity protected members, b) if using a reinforcement cage pin, the pin must be developed in both the column and the shaft, c) if using a pipe or solid steel pin, the pin must be developed in the shaft (Caltrans SDC).

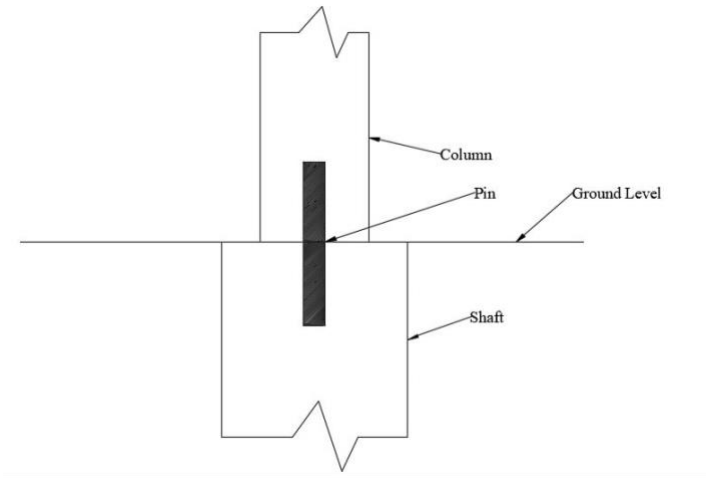

Figure 2.1. General Pin Connection

Restrained connections that transfer moment, shear, and axial force include a socket or drilled shaft connection, which uses RC for both the shaft and the column. This research will add another type using a direct connection between a CFST and a RC column.

The socket connection is dependent on the embedment of the column reinforcement cage into the pile-shaft and the transverse reinforcement in the shaft. A general socket connection diagram is shown in Figure 2.2. The difference between Type 1 and Type II shafts is that Type I shafts have an increased amount of concrete cover below ground, while Type II shafts have both an increased diameter and a separate reinforcement cage from the column.

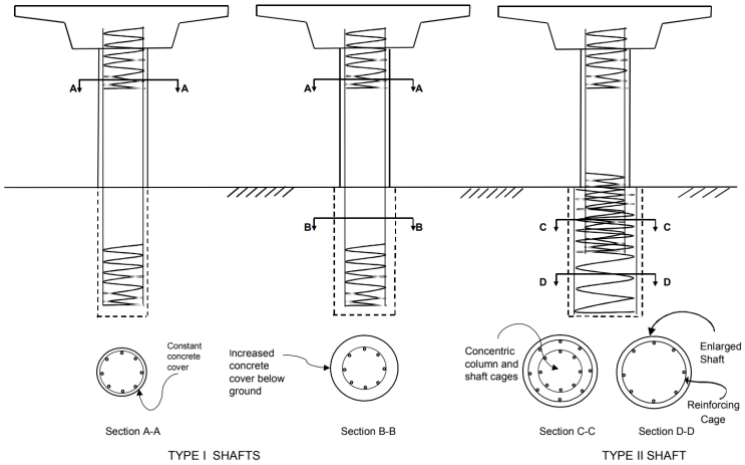

Figure 2.2. Column-Shaft Connection Types (Caltrans)

This connection also requires the shaft to be a capacity-protected member of the assembly, but Caltrans and WSDOT have differing requirements for the embedment length of the column reinforcement and the amount of required transverse reinforcement in the shaft.

Caltrans requires that the column longitudinal bar embedment length meet the following equation (Caltrans SDC Table 8.3.2-1):

$$l_e = \begin{Bmatrix} D_{c,max} + 42d_{bl} & for\ \#11\ bars\ and\ smaller \\ D_{c,max} + 48d_{bl} & for\ \#14\ and\ \#18\ bars \end{Bmatrix}$$

L_e = required embedment length of column longitudinal bar (in.)

$D_{c,max}$ = largest cross-sectional dimension of the column (in.)

d_{bl} = nominal diameter of column longitudinal bar (in.)

Caltrans requires the shaft transverse reinforcement to meet the following requirements based on a minimum volumetric ratio and maximum allowable spacing. This is shown in Table 2.2 (Caltrans SDC Table 5.4.5-1).

Table 2.2. Minimum Volumetric Ratio of Transverse Reinforcement in Caltrans Type II Shafts (Caltrans SDC)

Location	Minimum Volumetric Ratio of Transverse Reinforcement	
	CISS or CIDH with permanent casing	All other Shafts
Top 2 feet of Shaft	50% of that required at the base of the column	Same as that required at the base of the column
Between the bottom end of column cage and 2 ft. below the top of Type II shaft		50% of that required at the base of the column

WSDOT requires that the column longitudinal bar embedment length meet the following equation (WSDOT BDM 7.3.5):

$$l_e = l_s + e$$

l_s = the larger of $1.7l_{ac}$ or $1.7l_{d,c}$. The 1.7 factor represents a Class C lap splice modification factor from previous versions of AASHTO Bridge Design Specifications (BDS)

l_{ac} = development length (in.) from AASHTO Guide Specifications for LRFD Seismic Bridge Design (SGS) Section 8.8.4 for column longitudinal reinforcement (in.)

$l_{d,c}$ = tension development length from AASHTO BDS Section 5.11.2.1 for column longitudinal reinforcement (in.)

e = eccentricity distance between shaft and column longitudinal reinforcement (in)

WSDOT requires the shaft transverse reinforcement to meet the following equation (WSDOT BDM eq. 7.8.2-1), which is also used in AASHTO BDS:

$$\frac{A_{tr}}{s} = \frac{kA_l f_{u,l}}{2\pi f_{y,tr} l_s}$$

A_{tr} = area of transverse reinforcement (in.^{2})

S = spacing of the transverse reinforcement (in.)

k = factor representing the ratio of column tensile reinforcement to total column reinforcement at the nominal bending resistance

A_l = Total area of longitudinal column reinforcement (in.^{2})

$f_{u,l}$ = Specified minimum tensile strength of column longitudinal reinforcement (ksi)

$f_{y,tr}$ = the yield stress of the transverse reinforcement (ksi)

l_s = lap splice length of column reinforcement (in.)

A direct connection between a CFST shaft or pile and a RC column is also dependent on the embedment depth of the column longitudinal reinforcement but uses a ring or rib attached to the pile to help with the transfer of the moment. This connection, like the other, requires that the shaft be a capacity-protected element, and prior research has shown that a CFST element has significantly more strength than a similarly sized RC element. A general layout of a CFST-to Column connection is shown in Figure 2.3.

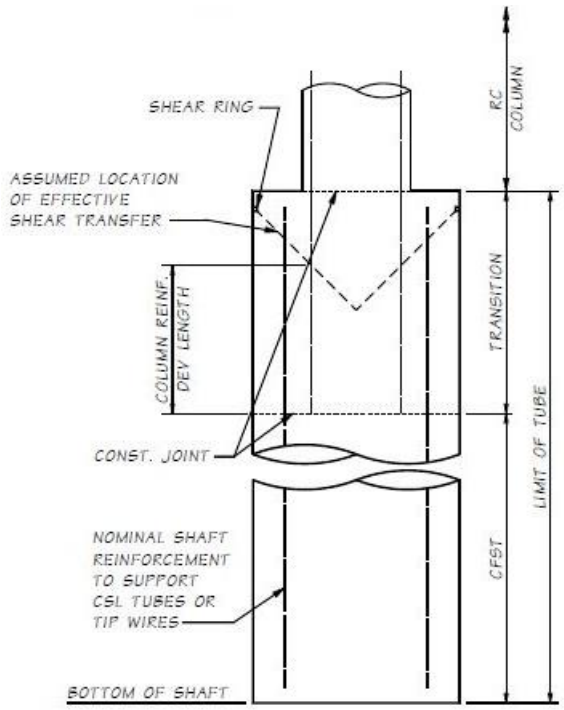

Figure 2.3. CFST-to Column Connection (WSDOT BDM)

WSDOT requires that a steel rib is welded to the inside of the steel tube 3 in. below the top of the tube and the column longitudinal bar embedment length meet the following requirements (WSDOT BDM 7.10.5):

$$l_e = maximum(0.5D + l_{d,bar}, 1.0D)$$

l_e = column longitudinal reinforcement embedment length (in.)

D = shaft diameter (in.)

$l_{d,bar}$ = column reinforcement development length (in.)

2.2 TEST PROGRAMS

Three different experimental test programs were reviewed to better understand the force-transfer mechanism used in the connection region and how the different study parameters affected the connection.

2.2.1 Lateral Behavior of RC Columns Supported on Type II Shafts: Liu (2012)

Liu (2012) tested two large-scale connections between an RC column and a Type II cast-in-drilled-hole (CIDH) RC pile as shown in Table 2.3 and completed a finite element (FE) analysis of the column-pile system under lateral load. The FE analysis studied the influence of the soil-structure interaction on the lateral behavior and how it would affect the test specimen configurations to simulate the behavior without using soil. The experiments exmined the column ductility capacity and the formation of the plastic hinge at the base of the column. TheAll specimens had a 4 ft. column diameter and 6 ft shaft diameter. The reinforcement of each specimen's column and shaft are shown in Figures 2.4 and 2.5. For both specimens, the shaft extends out of a RC footing, which is post-tensioned to the laboratory floor to prevent uplift. The

footing is 14-ft long, 8-ft wide, and 4-ft deep and designed to allow interface shear transfer between the base of the footing and the laboratory door.

Table 2.3. LIU (2012) Test Program

Specimen	Shaft Height	Column Height	Specimen Height	Column Reinforcement Development Length	Longitudinal Reinforcing Bar Size	Transverse Reinforcement Spacing (in)	Transverse Reinforcing Bar Size
1	9 ft.	16 ft.	29 ft.	7.5 ft.	#14	6, 5, and 4	#5
2	8 ft.	18 ft.	30 ft.	6 ft.	#18	6, 4, and 7	#5

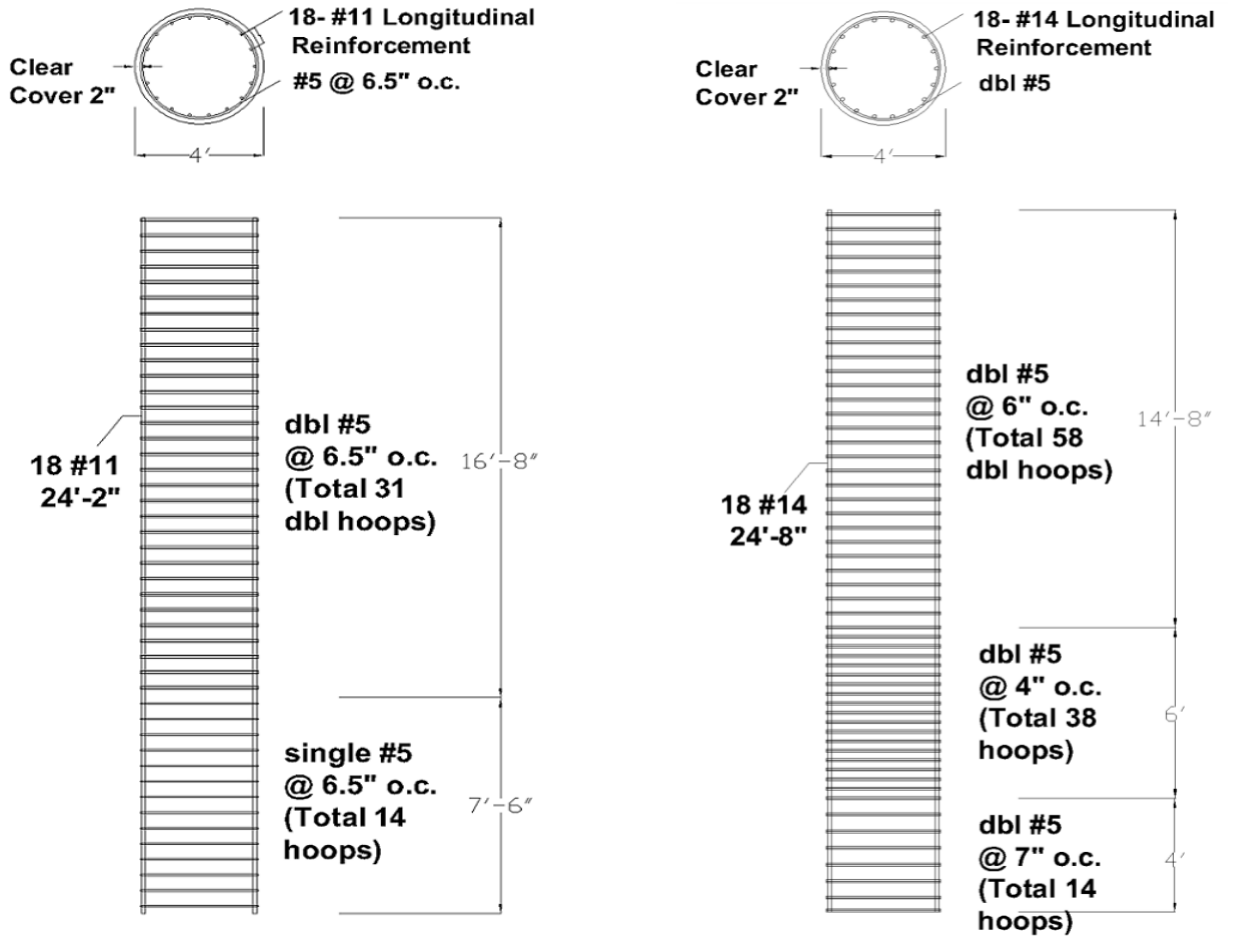

a) **b)**

Figure 2.4. Liu (2012) Column Reinforcement Cages: a) Specimen 1 and b) Specimen 2

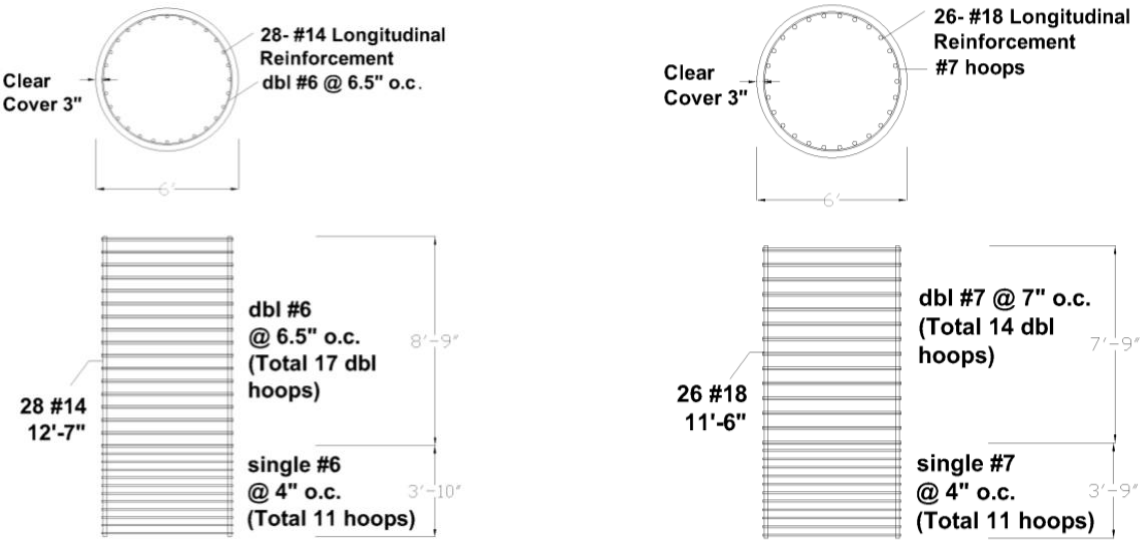

Figure 2.5. Liu (2012) Shaft Reinforcement Cages: a) Specimen 1 and b) Specimen 2

The specimens were post-tensioned to the laboratory floor to create a fixed base. The specimens were then loaded with a constant axial load and subjected to cyclic loading. Figure 2.6 shows the general test setup. The cyclic loading consisted of a lateral actuator subjecting the specimens to the prescribed force or displacement limit and returning the actuators back to the zero-force state. Specimen 1 reached a drift of 7% (+/-14 in.) and Specimen 2 reached a drift of 10.2% (+/-22 in.).

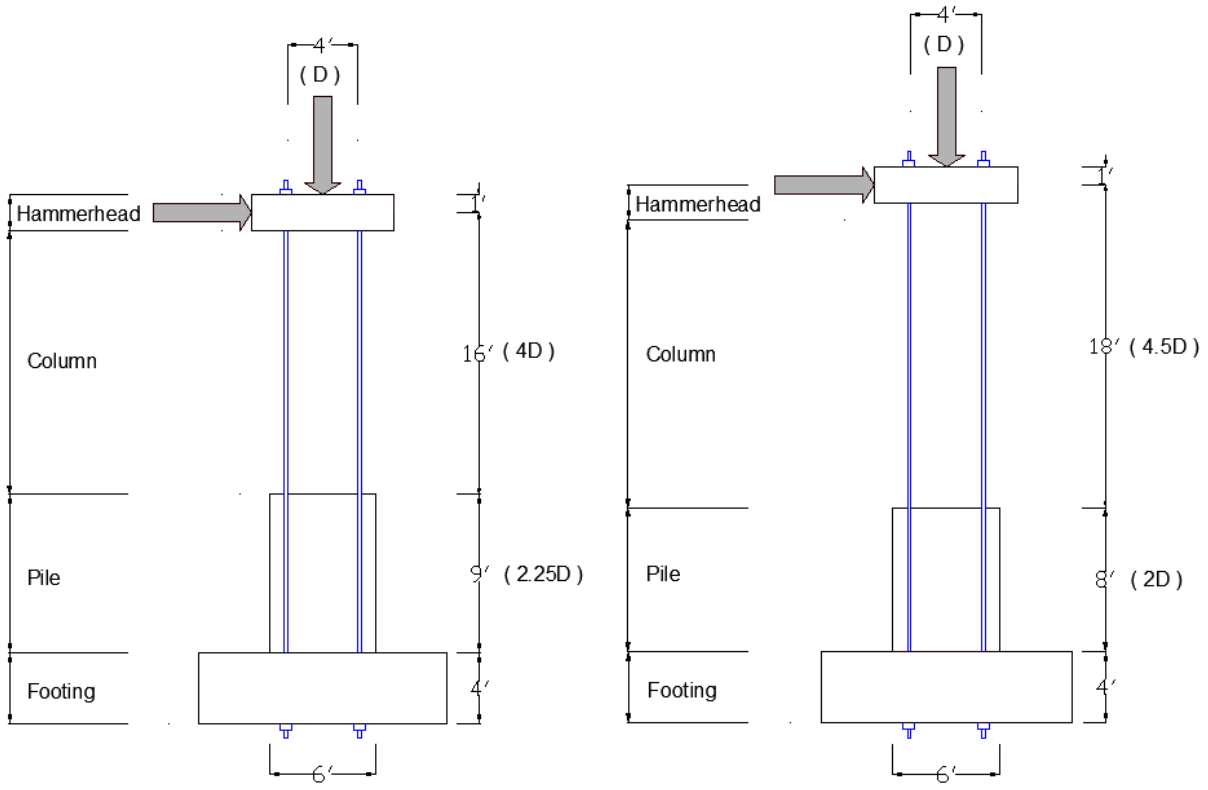

a) **b)**

Figure 2.6. Liu (2012) Test Setup: a) Specimen 1 and b) Specimen 2

Both tests were stopped after bar fracture occurred in the longitudinal reinforcement, shown in Figure 2.7. This occurred at cycle 14, (10.4 in. to -13.95 in.) for Specimen 1 and cycle 18 (21.54 in. to 22.46 in.) for Specimen 2.

a) b)

Figure 2.7. Liu (2012) Buckling and Fracture of Longitudinal Bars: a) Specimen 1 and b) Specimen 2

Figure 2.8 shows the force-displacement results of the two specimens. The specimens had similar results, with a loss in force after crushing and bar ruptures. Table 2.4 shows key ductility and strength values from the test.

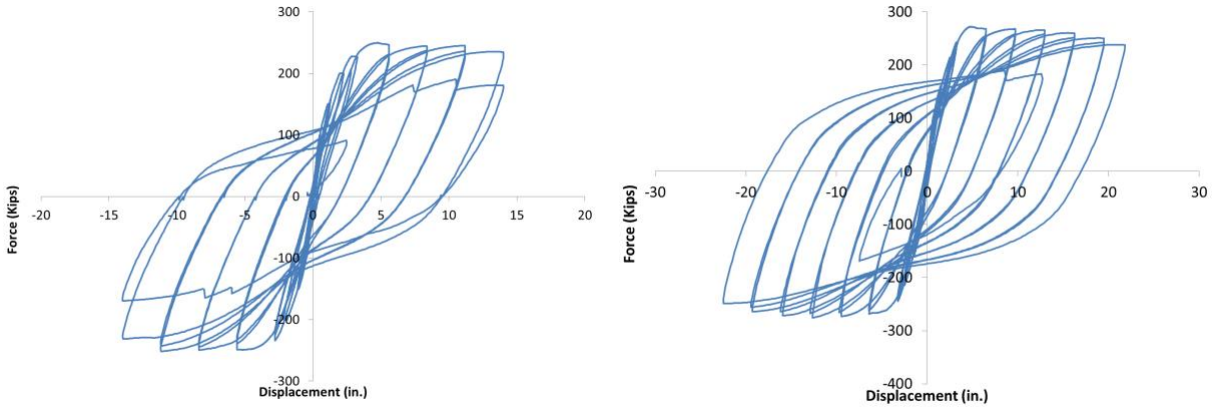

a) b)

Figure 2.8. Liu (2012) Overall Responses of Column-Shaft Assemblies including P-Δ Effects a) Test 1 and b) Test 2

Table 2.4. Displacement Ductility of the column-shaft assemblies (Liu 2012)

Specimen	First Yield Disp. (in.)		Effective Yield Disp. (in.)		Ultimate Disp. (in.)		Displacement Ductility (in./in.)		Peak Strength (kip)	
	Push	Pull	Push	Pull	Push	Pull	Push	Pull	Push	Pull
1	2.26	2.32	2.72	2.64	14.00	14.00	5.15	5.30	250	250
2	2.75	2.66	3.40	3.39	21.84	22.49	6.42	6.63	292	304

The relevant findings were as follows:

- The reduced embedment lengths, compared to current Caltrans standards, of the column reinforcing cages extending into the Type II shafts, is sufficient to fully develop the load resistance capacities of the columns
- The lateral displacements at the top of the columns were mainly contributed by column flexure (~50%) and base rotation (~40%) with the shear contribution (>5%) being negligible

2.2.2 Seismic Performance of Bridge Column-Pile-Shaft Pin Connections for Applications in Accelerated Bridge Construction: Mehraein (2016)

Mehraein (2016) investigated the seismic performance of two types of direct column-to-pile connections: (1) pipe-pin connections at column-pile shaft connections for CIP and precast constructions and (2) rebar-pin connections at column-pile shaft connections for CIP and precast constructions. Each Specimen would be tested with one precast column-pile and one CIP column-pile assembly, shown in Figures 2.9 and 2.10.

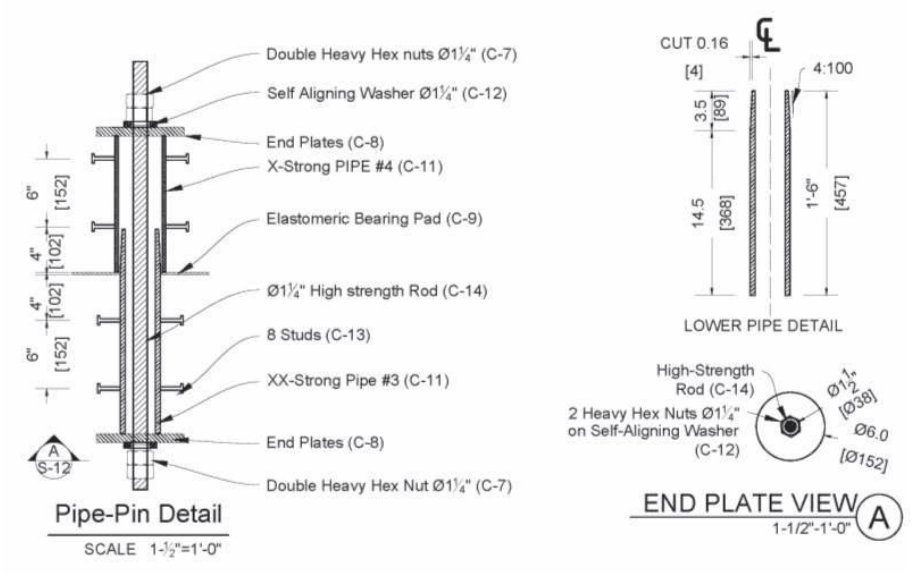

Figure 2.9. Mehraein (2016) BPSA Pipe-Pin Detail

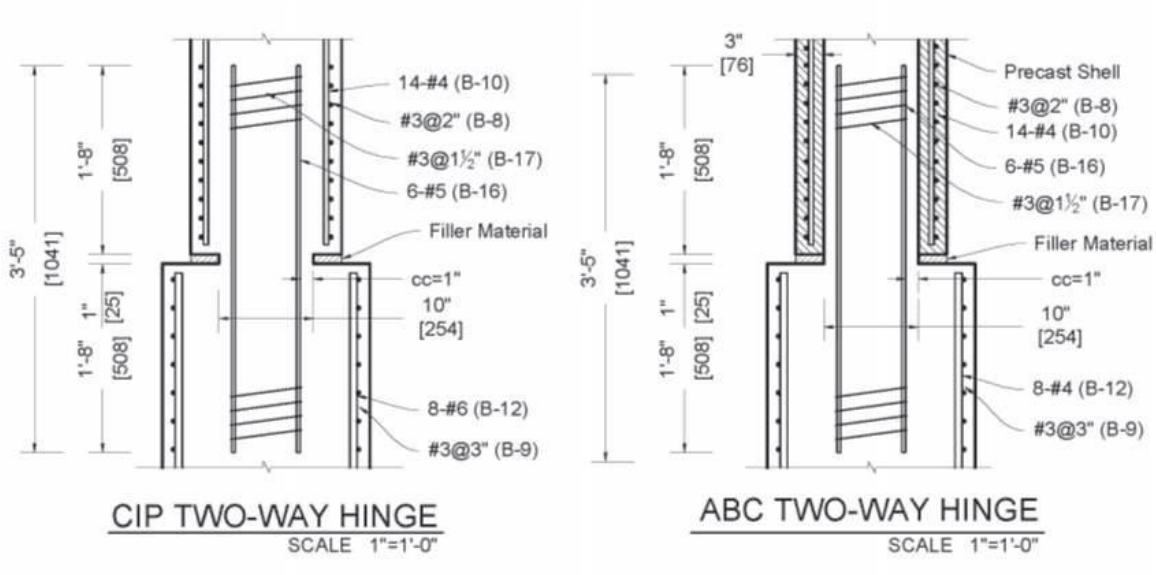

Figure 2.10. Mehraein (2016) BRSA Rebar Hinge Detail

Mehraein (2016) tested two 1/3.75 scale, two-column bent subassemblies, with one column as a precast shell filled with self-consolidating concrete and the other column being a Cast-In-Place concrete column, shown in Figures 2.11 and 2.12. The specifications and dimensions of the specimens are found in Table 2.5.

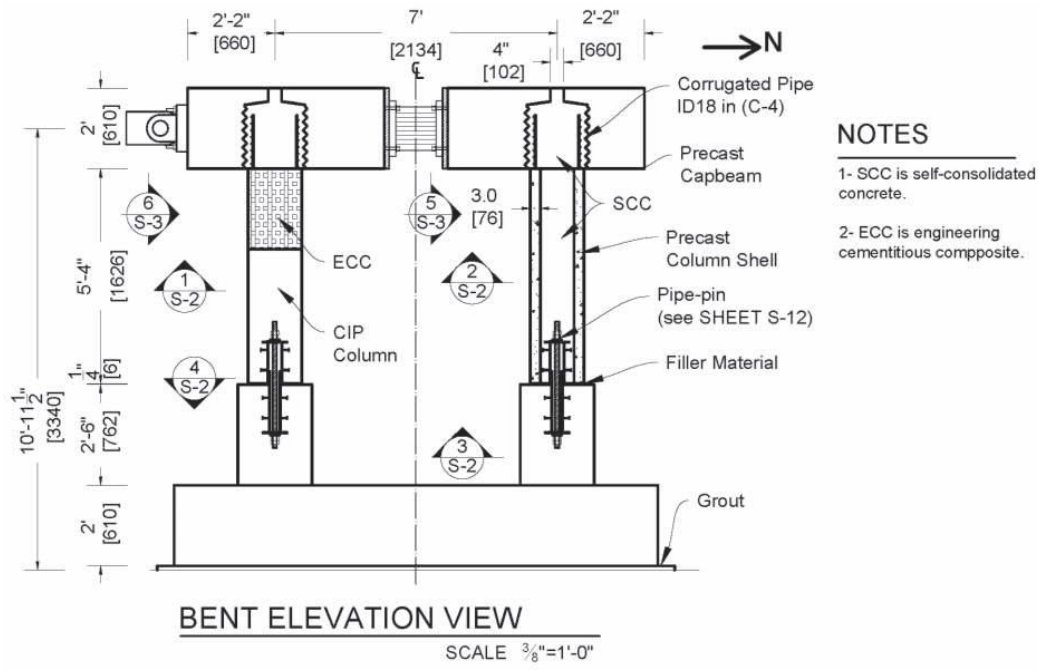

Figure 2.11. Mehraein (2016) BPSA Elevation View

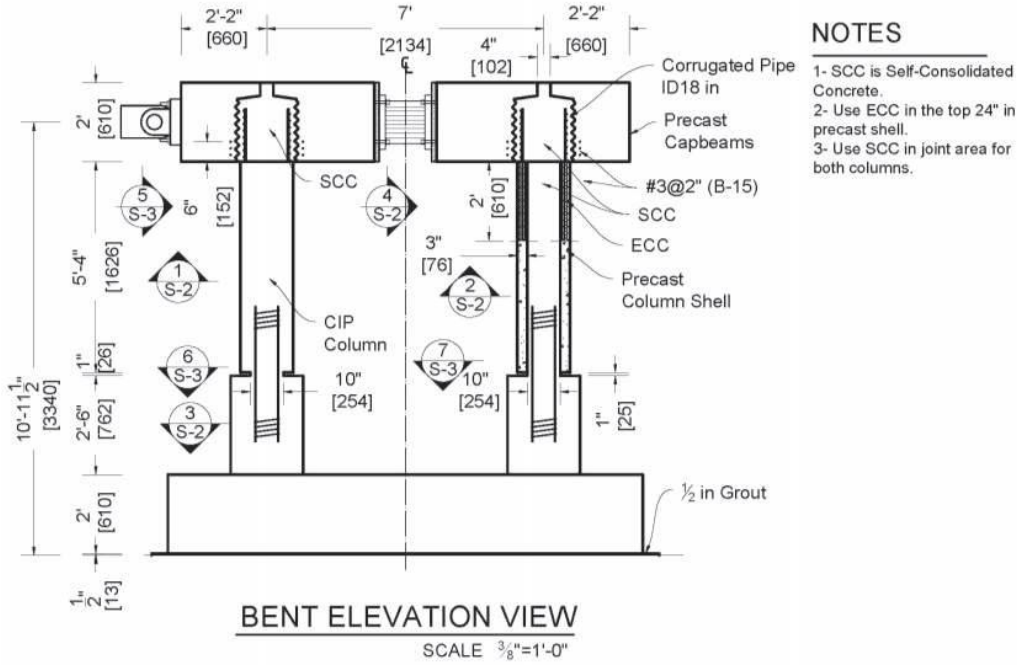

Figure 2.12. Mehraein (2016) BRSA Elevation View

Table 2.5. Mehraein (2016) Specifications of the Specimens

Model	BPSA	BRSA
Column Diameter	16 in.	
Column Longitudinal Reinforcement	14 - #4	
Column Spirals	W4 @ 2 in.	#3 @ 2 in.
Column Spiral Yield Strength	51 ksi	68 ksi
Pedestal Diameter	22 in.	
Pedestal Longitudinal Reinforcement	8 - #6	
Pedestal Spirals	#3 @ 3 in	

The specimens were subjected to the 142-degree of Sylmar Converter Station of the 1994 Northridge earthquake ground motions via a shake table as shown in Figure 2.13. The accelerations from these ground motions were filtered to create a symmetric ground motion and the time step of the acceleration was scaled to account for the specimen scale factor of 1/3.75. To account for the weight of the bent on the two columns, four blocks were placed on the mass rig. These four blocks on the mass rig provided the inertia force to the bent, a translational mass equivalent to 100 kips.

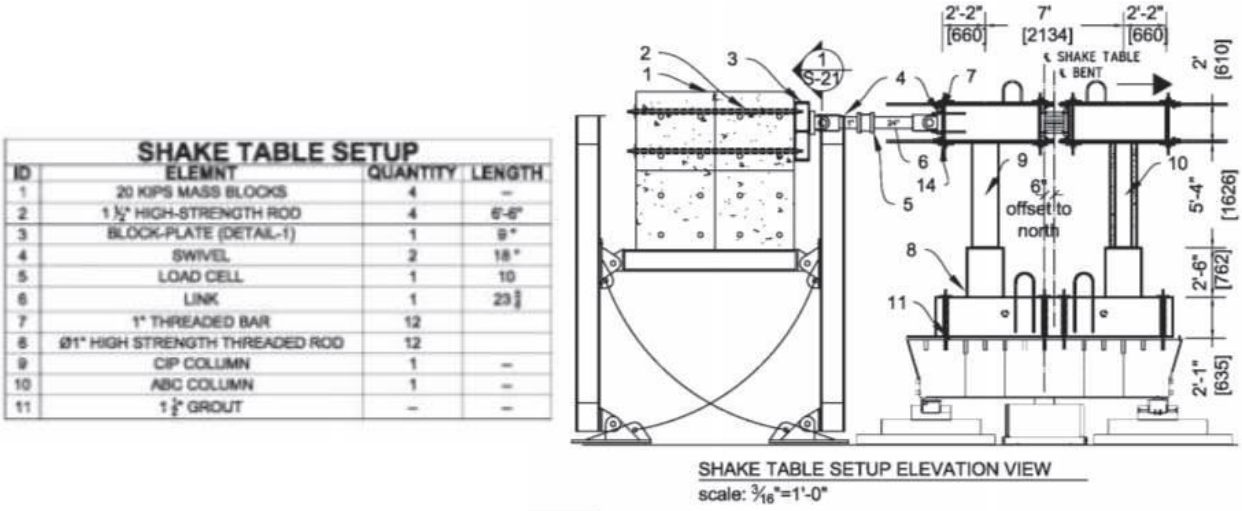

Figure 2.13. Mehraein (2016) Shake Table Setup

The BPSA specimen sustained 11 ground-motion runs before the test was terminated. The CIP components showed major cracking in the plastic hinge region of the column as well as buckled longitudinal reinforcement and ruptured spiral reinforcement. The pipe-pin had no

observable damage. The PC components had similar results, with major spalling and buckled reinforcement. The pipe-pin connection also showed no damage. The BPSA CIP force-displacement curve and the BPSA PC force-displacement curve are shown in Figure 2.14. The final state of the connection is shown in Figure 2.15.

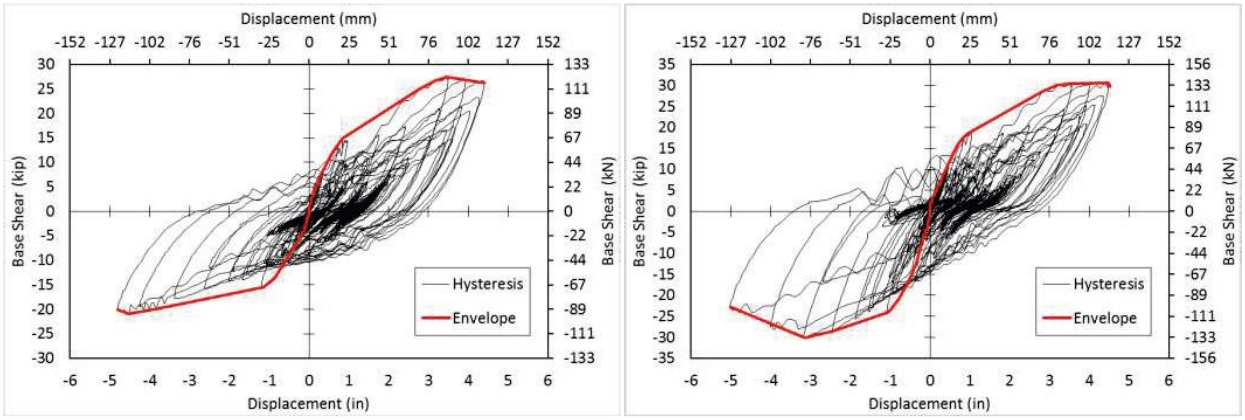

a) **b)**

Figure 2.14. Mehraein (2016) Force-Displacement Curve a) BPSA CIP and b) BPSA PC

a) **b)**

Figure 2.15. Mehraein (2016) BPSA Connection After Final Run a) CIP and b) PC

The BRSA specimen managed to do 6 ground-motion runs before the test was terminated. The CIP components showed major spalling at the top of the column. The concrete core of the

column failed after run 6. The longitudinal bars also buckled. The spalling also caused the rebar-pin spiral to be exposed. The PC components had shear and flexural cracks which expanded in size after each run. There was a large flexural crack in the rebar-pin, which occurred during run-5, but did not grow with the reaming runs. The BRSA CIP and the BRSA PC force-displacement curves are shown in Figure 2.16. The final state of the connection is shown in Figure 2.17.

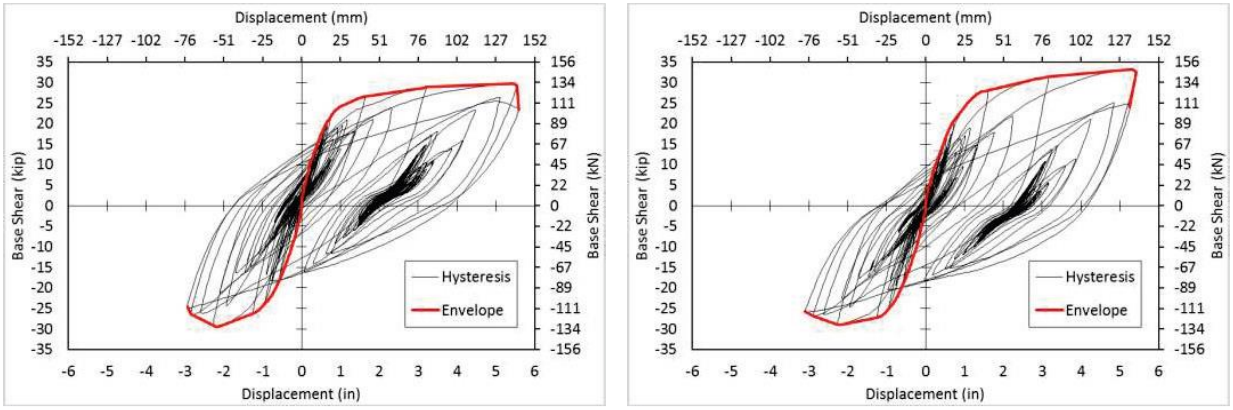

a) **b)**

Figure 2.16. Mehraein (2016) Force-Displacement Curve a) BRSA CIP and b) BPSA PC

a) **b)**

Figure 2.17. Mehraein (2016) BRSA Connection After Final Run a) CIP and b) PC

The relevant research findings are as follows:

- The design and detailing methods developed in this study for the reinforcing bar cage pins, pipe-pins, pocket connections, and the precast cap beams led to an effective ductile bridge bent.

- Moments were developed at both pin types, leading to an increase in the base shear by approximately 30%. Even the pipe-pins, without any tension members, and the rebar-pins, with very small core diameters, generated significant moments at the column base
- The damage in the pipe-pin connections was minimal because the strains in the pipes and longitudinal bars were well below the yield, and cracks in the column and pedestal were thin and few.
- The moment-rotation relationship of rebar-pins was stable even when the pins underwent large plastic deformations under many cycles of earthquake loading. The concrete near the hinge throat was damaged but the column and pedestal reinforcement did not yield near the rebar-pins.

2.2.3 Seismic Performance of Column to Drilled Shafts: Chang (2021)

Chang (2012) specifically investigated the effects of transverse reinforcement by testing a 1/3.6-scale column-shaft subassembly under cyclic lateral loading, following the work of Hung (2015) who tested three similar subassemblies. Table 2.6 provides the experimental test matrix. The specimens had a column diameter of 20 in., column height of 60 in., shaft height of 30 in., embedment length of column reinforcement of 26 in., and the transverse reinforcement in the plastic-hinge region of column consisted of gauge-3 wire at 1.25 in.

Table 2.6. Chang (2021) Test Program

Researcher	Specimen	Shaft Diameter	Column Long. Reinf. Quantity and Bar Size	Shaft Long. Reinf. Quantity and Bar Size	Shaft Transverse Rein. Bar Size and Spacing
Hung	DS-1	30	10 #5	30 #3	2 gauge-9 wire @ 3 in
	DS-2	30	10 #5	30 #3	gauge-9 wire @ 3 in
	DS-3	26	16 #5	24 #4	3 gauge-9 wire @ 3 in
Chang	DS-4	30	16 #5	24 #4	gauge-9 wire @ 3 in

The loading included an axial load of 10% of the nominal compressive strength of the column and a cyclic lateral load at the top of the specimen. Figure 2.18 shows the general test setup for each specimen. (This setup was also used in this test program). Each specimen failed at a specimen drift of approximately 10% and was defined as when the lateral load resistance dropped by more than 50%. The moment-drift curve of DS-4 is also presented in Figure 2.19

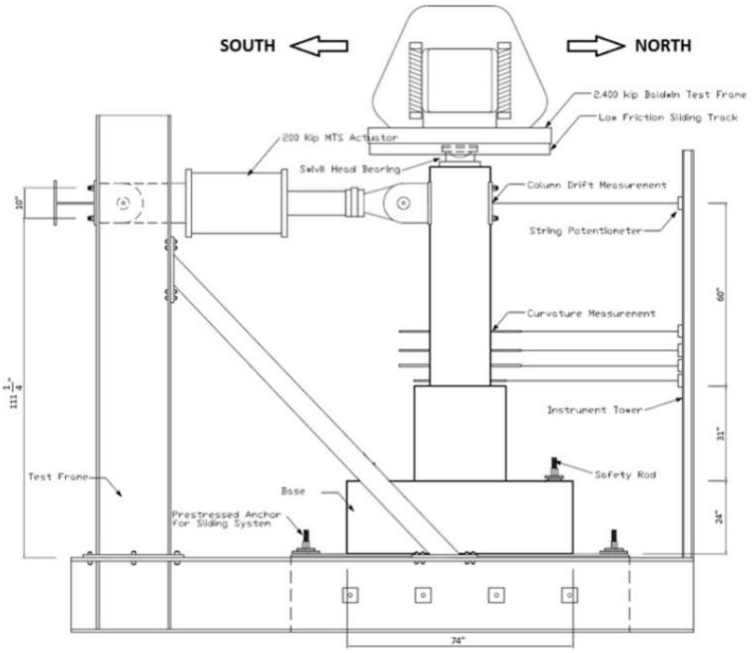

Figure 2.18. Chang (2021) Test Setup

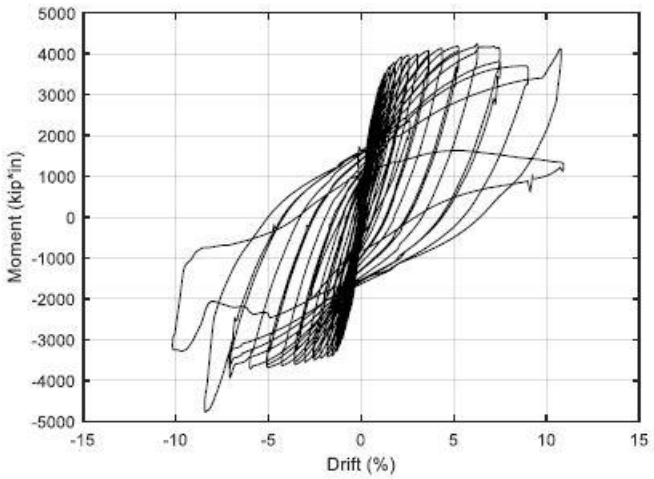

Figure 2.19. Chang (2021) Moment-Drift Response of DS-4

Specimens DS-1 and DS-3 failed by bar buckling and fracture in the column base. Specimen DS-2 and DS-4 failed due to prying occurring in the transition region, which is equivalent to the column embedment depth, the CIP concrete shell split open and the column was separated from the CIP shaft. The final states of these specimens are shown in Figure 2.20.

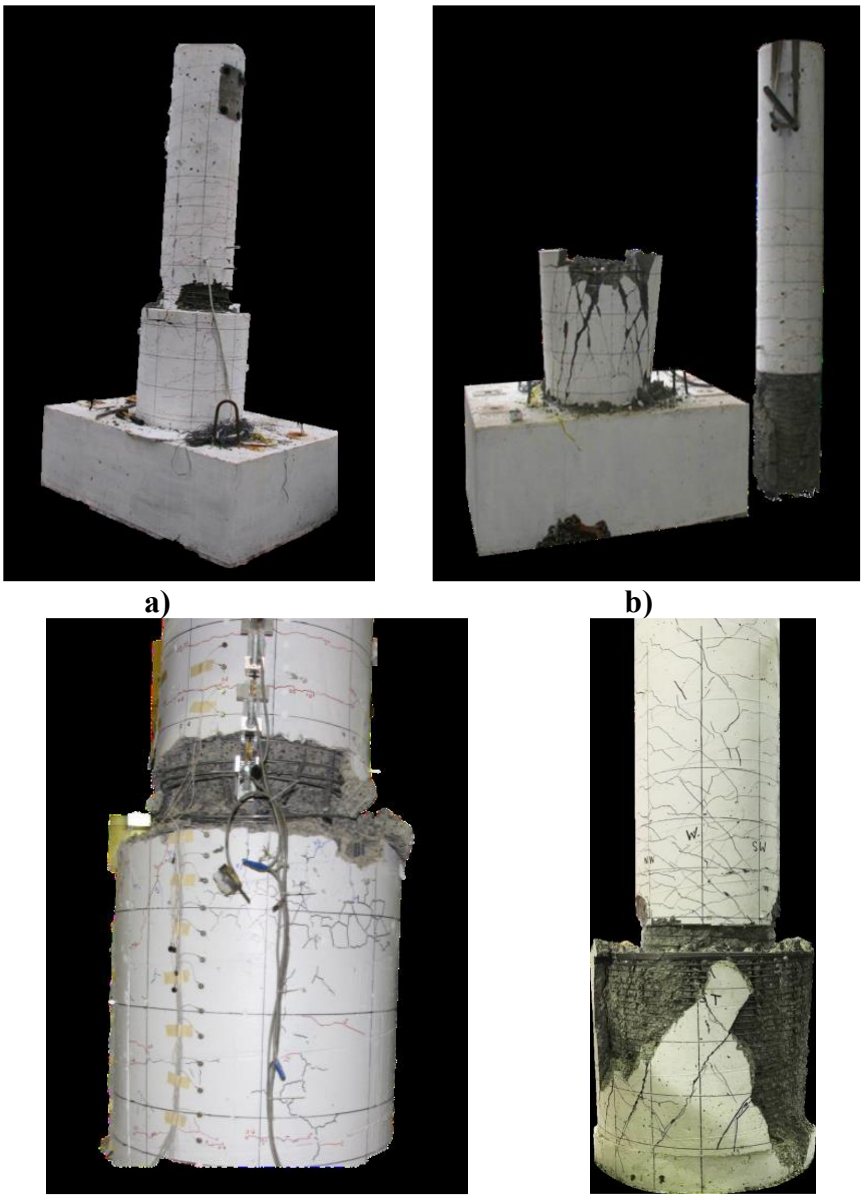

Figure 2.20. Final State of Specimens a) DS-1, b) DS-2, c) DS-3, and d) DS-4

The strain distribution in the shaft transverse reinforcement was not uniform throughout the specimens. The top regions of the spiral had a measured strain above the yield strain of the reinforcement, while the bottom spiral measured nearly zero strain.

The relevant findings were as follows:

- The current provisions (Caltrans and WSDOT) of the amount of spiral reinforcement required for conventional column-to-drilled shaft connections does not ensure the desired behavior for all configurations
- The amount of transverse shaft reinforcement can cause the failure mechanism to change from the column to the connection
- The tests specimens contained no external confining steel shell, such as a CFST, around the top of the transition region, and if one were used it would provide some of the benefits of additional spiral and may reduce the amount of spiral used

The research performed by Liu (2016), Mehraein (2016), and Chang (2021) provide some insight into the behavior of different column-shaft connections, as well as how various parameters affect the connection's behavior. Liu and Chang show that the majority of specimen deformation is due to base rotation and column flexure. Liu demonstrates that the embedment depth of column longitudinal reinforcement into RC shafts can be reduced, while still developing the capacity of the column. Mehraein showed that, while the pin type connection leads to an effective bridge bent with minimal damage, moments are developed at both pin types, which leads to an increase in the base shear. Chang emphasizes the importance that shaft transverse reinforcement has on the type of failure for an RC drilled shaft, and the benefits that a CFST would have on such a connection.

2.3 CFST CONNECTIONS

Prior research into the connections between CFST element and RC elements has shown to develop a full-strength connection between a tube and an RC element, such as a cap beam or a footing, requires an additional mechanical mechanism. Research programs performed at Montana State University (MSU) and the University of Washington (UW) studied these connections.

2.3.1 Performance of Steel Pipe Pile-to-Concrete Cap Connections Subjected to Seismic or High Transverse Loading: Kappes (2013)

The research performed by Kappes (2013) at MSU investigated the strength of an embedded CFST column-to-pier cap connection, as shown in Figure 2.21. This was done by extending the tube into the pier cap without the addition of a supplemental mechanical mechanism to enhance the bond between the two structural components. The key parameters of these tests were the CFT embedment length into the pile and the strength of the pile cap concrete.

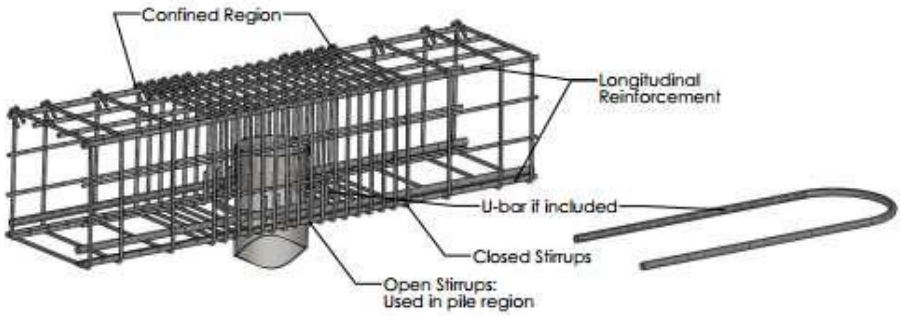

Figure 2.21. CFST to Pier Cap Connection (Kappes 2013)

Six ½ scale specimens were tested to evaluate the strength of the connection. Four specimens were subjected to monotonic loading to determine the ultimate strength of the connection. The other two specimens were tested under cyclic loading to determine the performance under multiple cycles of increasing load. Table 2.7 provides the experimental test

matrix with the key parameters being investigated, Pile thickness, embedment length, and concrete strength. The RC pile cap, which was the same for all specimens, was 18 in. by 18 in. by 68 in. All the CFTs used had an outside diameter of 8.625 in.

Table 2.7. Kappes (2013) Test Program

Specimen	Loading	Pile Thickness	Embedment Length	Design Concrete Strength
VT1	Monotonic	0.25 in.	9.0 in.	6.25 ksi
VT2	Monotonic	0.50 in.	11.75 in.	4.0 ksi
VT2.5	Monotonic	0.50 in.	9.0 in.	6.25 ksi
VT3	Monotonic	0.50 in.	10.375 in.	4.0 ksi
CT1	Cyclic	0.73 in.	11.75 in.	4.0 ksi
CT2	Cyclic	0.73 in.	11.75 in.	4.0 ksi

As mentioned previously, these connections were tested under monotonic and cyclic loading by applying lateral loads and a constant axial load of 15 kips to represent gravity loads through hydraulic jacks, as shown in Figure 2.22. The monotonic tests were loaded in the positive direction until a distinct loss in load-carrying capacity was observed. The process was then repeated to the same deflection in the negative direction. The maximum drifts reached for VT1, VT2, VT2.5, and VT3 are approximately 14%, 15%, 15%, and 14.5%, respectively. The cyclic tests were tested by displacing the pile over increasing drift cycles up to 11% drift.

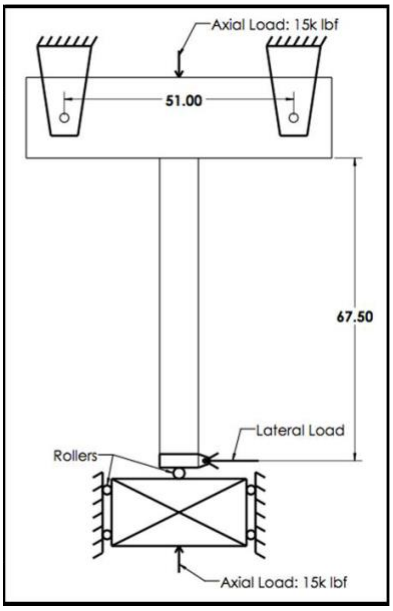

Figure 2.22. General Test Setup Layout (all lengths in units of in.) (Kappes 2013)

Specimen VT1 failed due to the formation of a plastic hinge in the CFT pile while all the other specimens failed due to fracturing in the pile cap. This change in failure mechanism is due to VT1 having a significantly smaller CFT. A summary of the test results is shown in Table 2.8.

Table 2.8. Kappes (2013) Summary of Test Results

	Test	U-bar Configuration	U-bar Location	Pile Embedment Length	Concrete Strength	Failure Mechanism	Maximum Moment at Failure
Monotonic	VT1	Single #7 U-bar in each direction	Exterior Only	9.0 in	6250 psi	Plastic hinge in steel pipe pile	119.2 ft·kip
	VT2	Single #4 and #5 U-bar in each direction	Exterior Only	11.75 in	3800 psi	Fracture of the concrete pile cap	173.8 ft·kip
	VT2.5	Single #7 U-bar in each direction	Exterior Only	9.0 in	6250 psi	Fracture of the concrete pile cap	138.5 ft·kip
	VT3	Single #7 U-bar in each direction	Exterior Only	10.375 in	4100 psi	Fracture of the concrete pile cap	151.7 ft·kip
Cyclic	CT1	Single #4 and #5 U-bar in each direction	Exterior Only	11.75 in	4200 psi	Fracture of the concrete pile cap	172.4 ft·kip
	CT2	Single #4 and #5 U-bar in each direction	Interior and Exterior	11.75 in	4200 psi	Fracture of the concrete pile cap	181.8 ft·kip

The final states of Specimen VT1 (plastic hinge) and CT2 (pile cap fracture) are shown in Figure 2.23. The moment-drift behavior of CT2 is shown in Figure 2.24.

a) **b)**

Figure 2.23. Final State of Specimens a)VT1 b) CT2 (Kappes 2013)

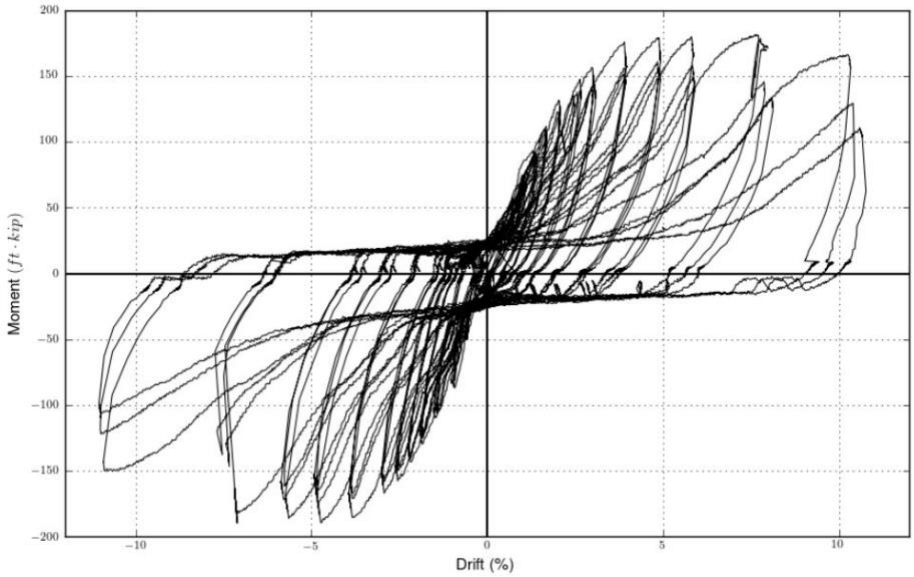

Figure 2.24. Moment-Drift of Specimen CT2 (Kappes 2013)

The relevant finding was as follows:

- An increase in the embedment depth of the CFT into the pile cap would reduce concrete crushing in the pile cap and increase the moment capacity of the column

2.3.2 Design Expressions and Dynamic Evaluation of CFST Bridges Subjected to Seismic Hazards: Stephens (2016)

The research performed by Stephens (2016) focused on connections capable of developing teh full plastic-moment capacity of a CFST component to a RC component. Stephens investigated three types of connections for a CFST column into a RC cap beam: a) Embedded Ring (ER), b) Welded Dowel (WD), and c) RC (RC), as shown in Figure 2.25. The ER connection uses a circular ring welded to the end of the tube that extends both inside and outside the tube. Four ER specimens were tested. The WD connection uses a ring of headed dowels, which are welded directly to the tube that extends into the cap beam. Three WD specimens were tested. The RC connection uses a

reinforcing cage, with both longitudinal and transverse reinforcement, which extends from the CFST into the cap beam. Only one RC specimen was tested.

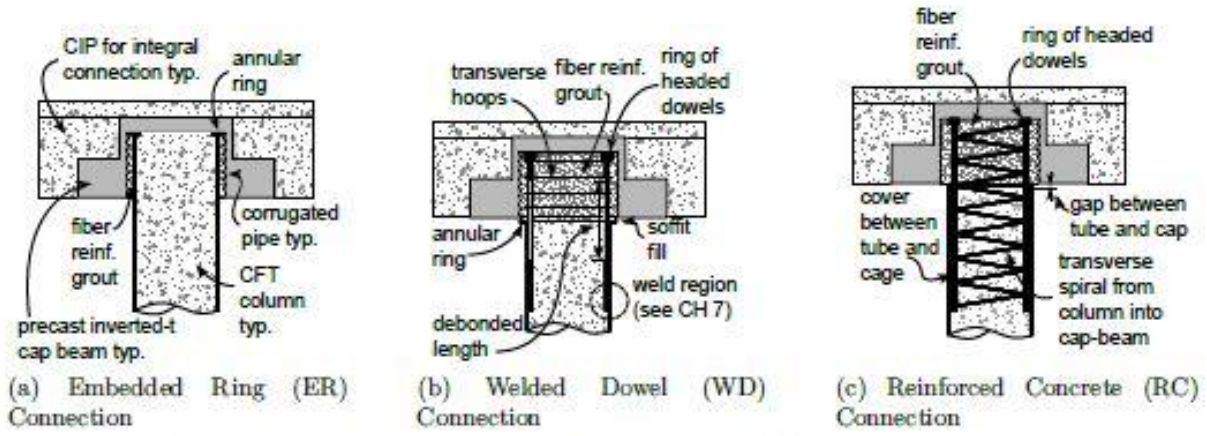

Figure 2.25. CFST to Pier Cap Connections (Stephens 2016)

The specimens were tested under axial and lateral loading similar to Chang's and this research's test program. The axial load was either 10% or 5% of the column capacity. The lateral loading was imposed displacement based on the column's yield displacement.

The ER connection was able to reach large strength, stiffness, and deformation capacities. The maximum drifts reached at 20% lateral strength degradation of the column ranged from 5% to 8.6% drift. The moment-drift behavior of the ER connection is shown in Figure 2.26. All ER connection specimens reached the plastic moment capacity of the CFST component. The failure mode for all specimens was ductile tearing at the column-to-cap beam interface. The ER connection has the advantage of reduced on-site construction time since no additional reinforcement is required.

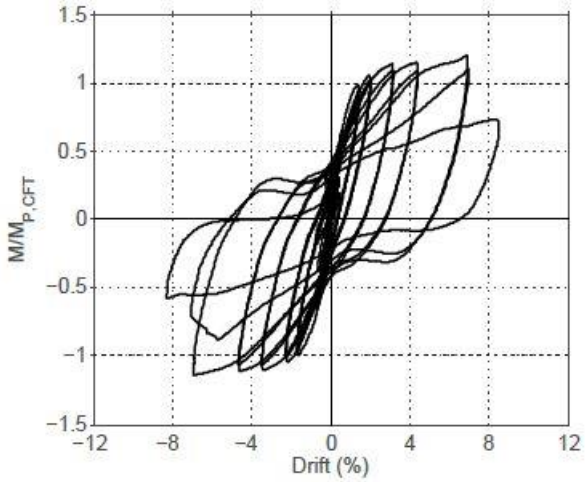

Figure 2.26. Moment-Drift Behavior of ER Connection (Stephens 2016)

The WD connection was also able to reach large strength, stiffness, and deformation capacities, however, the capacities were controlled by the effective reinforcing ratio of the dowels and therefore were smaller capacities than a comparable ER connection. The maximum drifts reached at 20% lateral strength degradation of the column ranged from 11.5% to 12.2% drift. The moment-drift behavior of the WD connection is shown in Figure 2.27. The two failure modes for this type of connection were cap beam failure due to the pullout of the headed dowels and yielding and fracture of the longitudinal dowels. The WD connection requires more on-site construction and labor and is not advantageous for accelerated construction.

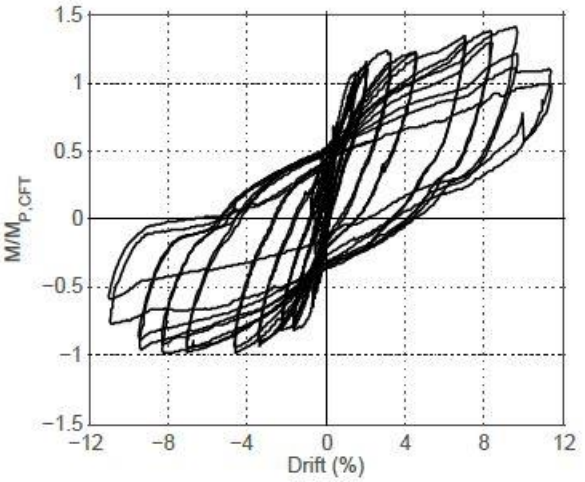

Figure 2.27. Moment-Drift Behavior of WD Connection (Stephens 2016)

The RC connection showed significantly lower strength and stiffness than the CFST component. The maximum drift reached at 20% lateral strength degradation of the column was 10% drift. The moment-drift behavior of the RC connection is shown in Figure 2.28The failure mode of this connection was the yielding and fracturing of the longitudinal reinforcement between the CFST and the cap beam. The RC connection is also not advantageous for accelerated construction due to the reinforcing cage that must be built on-site.

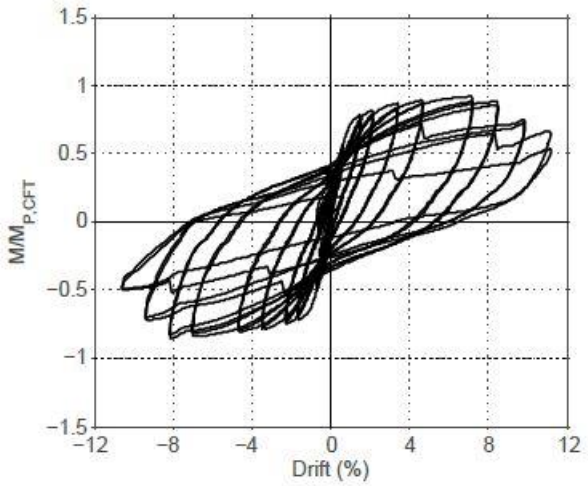

Figure 2.28. Moment-Drift Behavior of RC Connection (Stephens 2016)

The relevant findings are as follows:

- There is an increase in time and labor used for the construction of an RC or WD connection compared to the ER connection
- The ER connection showed improved seismic performance in ductility and strength compared to the RC and WD connections
- For the WD connection, extending the longitudinal dowels into the CFST would improve performance and steel stress distribution, and prevent damage to the tube

The research performed by Kappes (2013) and Stephens (2016) highlights the benefits of increased embedment depth and the addition of a rib into a CFST connection. The increased

embedment depth helps to develop the full capacity of the CFST member and the rib provides the tube with additional anchorage to the RC component and creates a strut for the reinforcing bars.

Chapter 3. EXPERIMENTAL TEST PROGRAM

Two half-scale CFST Pier to Pile connection specimens were tested to assess the cyclic, nonlinear response of the proposed connections. The RC column was identical for all of the specimens, while the pile varied between the different specimens. This chapter presents the dimensions, reinforcements, and measured material properties of each specimen. The experimental test apparatus, loading, and instrumentation are described also.

3.1 Design and Construction of Test Specimens

The specimens were designed to represent a 40 in. diameter RC prototype bridge column with a 5 ft. or an 8 ft. diameter CFST pile. A scale factor of ½ was used due to the constraints of the available testing equipment, available materials, and prior analytical research (Zhao 2020) done on these connections. The first specimen, Specimen 30-21, is a 30 in. diameter pile with a column reinforcement embedment depth of 21 in., the AASHTO development length of a #7 Reinforcing steel bar. The second specimen, Specimen 48-21, is a 48 in. diameter pile with a column reinforcement embedment depth of 21 in. The test matrix is shown in Table 3.1.

Table 3.1. Specimen Test Matrix

Specimen Name	Tube Diameter (in.) [mm]	Tube Diameter/ Tube Thickness	Reinforcement Bar Size	Embedment Depth (in.) [mm]	Rib Size (in.) [mm]	Rib Embedment Depth (in.) [mm]
30-21*	30 [762]	60	#7	21 [533]	NA	NA
48-21	48 [1219]	96	#7	21 [533]	NA	NA

*Specimen 30-21 is reference specimen

The specimen RC columns have the same dimensions and layout as shown in Figure 3.1. The total column length was 74 in., including the 12.25 in. extending above the point of lateral loading, but does not include the 21 in. embedment depth of the column reinforcement into the pile, and. The top 30 in. of the column was replaced with a 20 in. diameter, 0.375 in. thick steel tube, filled with concrete to prevent damage to the RC column unswe laterally loading during testing without affecting the performance of the connection zone.

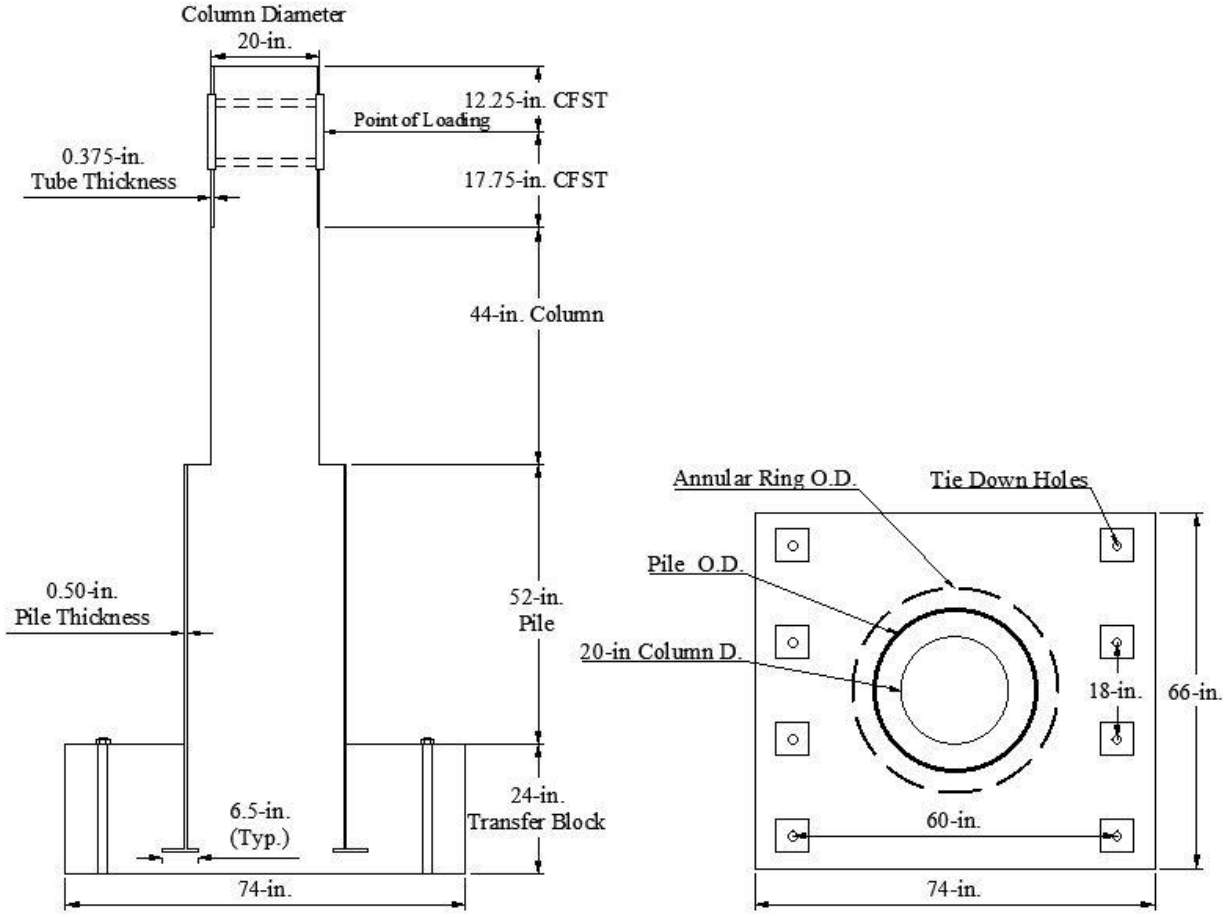

Figure 3.1. Specimen Layout and Dimensions a) Cross-section view b) Plan view

The test specimen for this research consisted of the RC column and the connection to the CFST pile. The pile had a diameter of 30 in. for Specimen 30-21 and 48 in for Specimen 48-21. All the tubes used for the piles had a thickness of 0.5 in, resulting in a D/t ratio of 60 for the 30 in. diameter tubes and 96 for the 48 in. diameter tube. The total tube length was 71.5 in. which

included the bottom 19.5 in. embedded into the transfer block. A normal-strength steel (50 ksi yield stress) annular ring, 6.5 in wide by 0.5 in. thick, was welded to the base of each pile using a fillet weld. The rings projected 4 in. on the outside of the pile and 2 in. on the inside of the pile.

The force and moment transfer between the column and the CFST pile is the behavior of interest. The pile was embedded in a 74" x 66"x 24" RC transfer block which anchored the specimen to the test rig. The embedment depth of 19.5 in. and annular ring were chosen to assure the CFST pile could develop the required resistance without damage block and was based on previous research (Stevens 2015). The transfer block (see Fig. 2.2) was designed to remain elastic throughout the test and adapt to the anchor points and dimensions of the test rig. A total of eight tie-down rods were used, four on each side. The tie-down rods were 1 ¼-in Williams Form Engineering All-Thread high-strength steel bars.

The test specimens were constructed simultaneously in two phases. The transfer blocks were constructed first. While building the reinforcement cage, the locations of the testing rig tie-downs were accounted for by placing 2.875" diameter PVC pipes at the locations where the tie-down rods would be anchored.

The steel tube sections for the CFST pile were cut to a length of 71.5 in. on-site from a straight seam welded tube using an oxy-acetylene torch. The cut ends were ground down smooth and annular rings supplied by a professional steel fabrication shop were then fillet welded to the tubes by a certified welder. For Specimen 30-21 the fillet weld size was 0.625 in. and for Specimen 48-21 the fillet weld size was 0.5 in. On the outside flanges on the ring, 1.25 in. holes were drilled. Support screws were then tack welded through these holes to act as supports to hold the base of pile 4 in. above the base of the transfer block.

The RC column reinforcement was consistent with WSDOT standards and consisted of 14 evenly spaced #7 steel bars, with a transverse reinforcement of 23 #3 hoops spaced at 3 in. in the

plastic region of the column and spaced at 5 in. in the elastic region of the column. The column longitudinal reinforcement and strain gauges were mounted at select locations. The transverse reinforcement was then tied into place along the length of the column and the ends of the hoops were bent so that there was a 90-degree seismic hook at both ends of the hoop around the longitudinal reinforcement. The column reinforcement cage was then placed inside the pile, resting on rods such that the reinforcement was the correct depth, 21 in., inside the pile as shown in Figure 3.4.

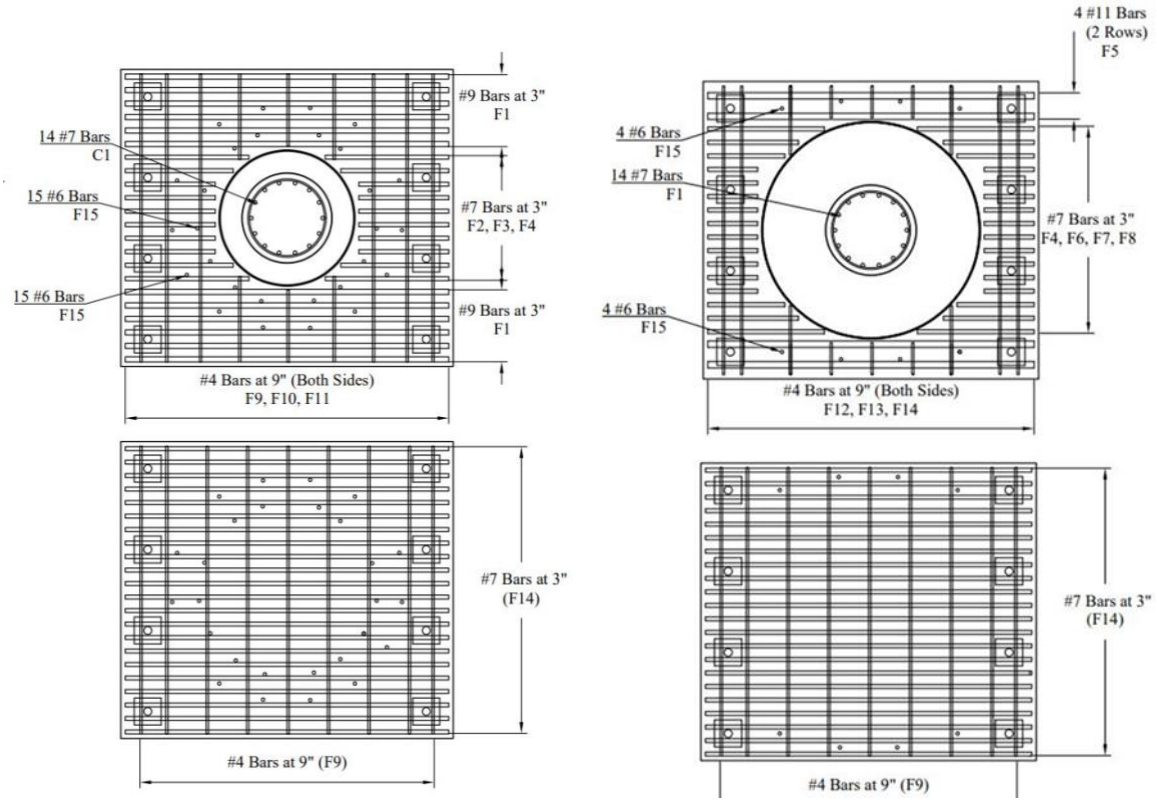

Figure 3.2. Transfer Block Reinforcement a) Specimen 30-21 and b) Specimen 48-21

Figure 3.3. Specimen 30-21 Reinforcement

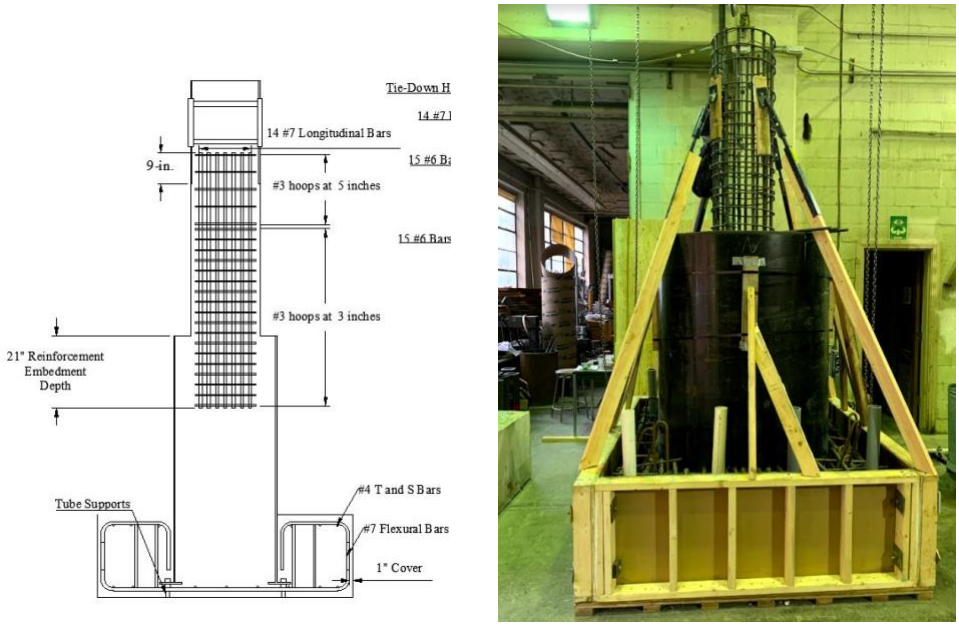

a) **b)**

Figure 3.4. Specimen Reinforcement a) Specimen Elevation and Reinforcement and b) Specimen 48-21 Completed Reinforcement Cage

A concrete mix design for structural applications (6000-A) was cast using a concrete pump truck. For Specimens 30-21, the first cast was the transfer block and the RC column up to the top of the pile. Wet burlap was placed on the exposed concrete to optimize curing. A Sonotube was then placed as formwork for the column and the second cast completed the specimen. This was done the top CFST were placed and secured around the exposed column reinforcement. The concrete was cured before testing.

For Specimen 48-21 the first cast was the transfer block of the specimen. This cast used a self-consolidating concrete (SCC) mix as a different cast was being performed in the lab and the mix met the compressive strength requirements that the transfer block. The second cast used the same mix as the other specimens (6000-A) and consisted of filling up the remaining height of the pile. A Sonotube formwork was placed and the third cast formed the column. The concrete was cured before testing.

3.2 SPECIMEN MATERIALS

Specimen materials are summarized in Table 3.2, along with their respective specifications and supplying vendors.

Table 3.2. Material List

Item	Designation	Vendor
Concrete	6000-A, 4-ksi	Stoneway Concrete
Reinforcing Steel	A 706 Grade 60	Addison Supply
Straight Seam Steel Tubes	API 5L	Richards Pipe

3.2.1 Concrete

A total of eight casts were done. Two separate casts for Specimen 30-21. Three separate casts for Specimen 48-21. A total of three casts for Specimens 30-21-R and 30-21-LD, each one had a single cast separately and shared one cast.

Concrete was ordered from a single ready-mix plant in the Seattle area. A 4000 psi mix was specified with ¾ in. aggregate passing. For each cast, 4 in. by 8 in. cylinders were made to track the strength of the concrete as it cured and for Day of Test material properties. The transfer block was to remain elastic and only compressive cylinders were made of these cylindere. Casts that were used for the pile only compressive strength and tensile strength cylinders were made. For casts that were used for the column compressive strength, tensile strength, and elastic modulus cylinders were made.

All the test cylinders were stored in a calcium hydroxide water bath, per ASTM C511, until the various tests were performed. Cylinders used for elastic modulus tests were sulfur capped to ensure parallel loading surfaces. Compressive tests, splitting tensile tests, and elastic modulus tests were performed per appropriate ASTM standards as shown in Figure 3.5. The results of the compression, splitting tensile, and elastic modulus tests are summarized in Table 3.3.

Table 3.3. Day of Test Concrete Properties

Specimen ID	Mean Compressive Strength (psi)			Mean Splitting Tensile Strength (psi)		Mean Elastic Modulus (psi)
	Transfer Block	Pile	Column	Pile	Column	Column
30-21	8957		6742	526	431.9	4529
48-21	12040	5455	5127	402.1	432.4	4121

a) **b)** **c)**

Figure 3.5. Tested Concrete Cylinders in a) Compression, b) Tension, and c) Elastic Modulus

Reinforcing bars were purchased from Addison Construction Supply in Tacoma, Washington. The bars were A706 Grade 60 and it was requested that all reinforcement of the same size and grade be from the same heat.

The reinforcement was expected to yield from the lateral loading during the test. To determine the actual stress-strain relation of the reinforcement, steel from the longitudinal column reinforcement was tested in tension to ASTM 370 standards. The test setup is shown in Figure 3.6. The stress-strain relationship of the reinforcement was characterized using the stress and strain at the Yield, Ultimate, and Fracture points, which are shown in Table 3.4 below.

Table 3.4. Longitudinal Reinforcement Material Properties

	Specimens 30-21 and 48-21	
	Average Stress (ksi)	**Average Strain**
Yield	70	.0024
Ultimate	106.2	.06
Fracture	77.8	.155

Figure 3.6. Reinforcement Tensile Test Setup

The straight seam welded steel tubes are API 5L X52 for the 30 in. diameter tube, a 52 ksi nominal yield strength, and API 5LB X42 for the 48 in. diameter tube, a 42 ksi nominal yield strength. Tubes were purchased from Richards Pipe & Steel, Inc. in Pacific, Washington.

a) **b)**

Figure 3.7. a) 48 in. and b) 30 in. Diameter Steel Tubes Cut to Size

The rings were purchased from and manufactured by Bloch Steel in Seattle, Washington. They are A572 Gr. 50 steel. The rings were fillet welded to the tubes using a 5/64 in. diameter Coreshield 8 E70 welding electrode. All structural welding was performed by a certified welder.

Figure 3.8. Annular Rings for Specimens 30-21 and 48-21

3.3 EXPERIMENTAL TEST SETUP

Figure 3.9 illustrates the test setup. Lateral loads were applied using a combination of an MTS Actuator and a self-reacting test rig and axial loads were applied using a 2400-kip Baldwin Universal Testing Machine using a spherical bearing. The MTS Actuator has a capacity of 220 kips and a maximum stroke of +/- 10 in.

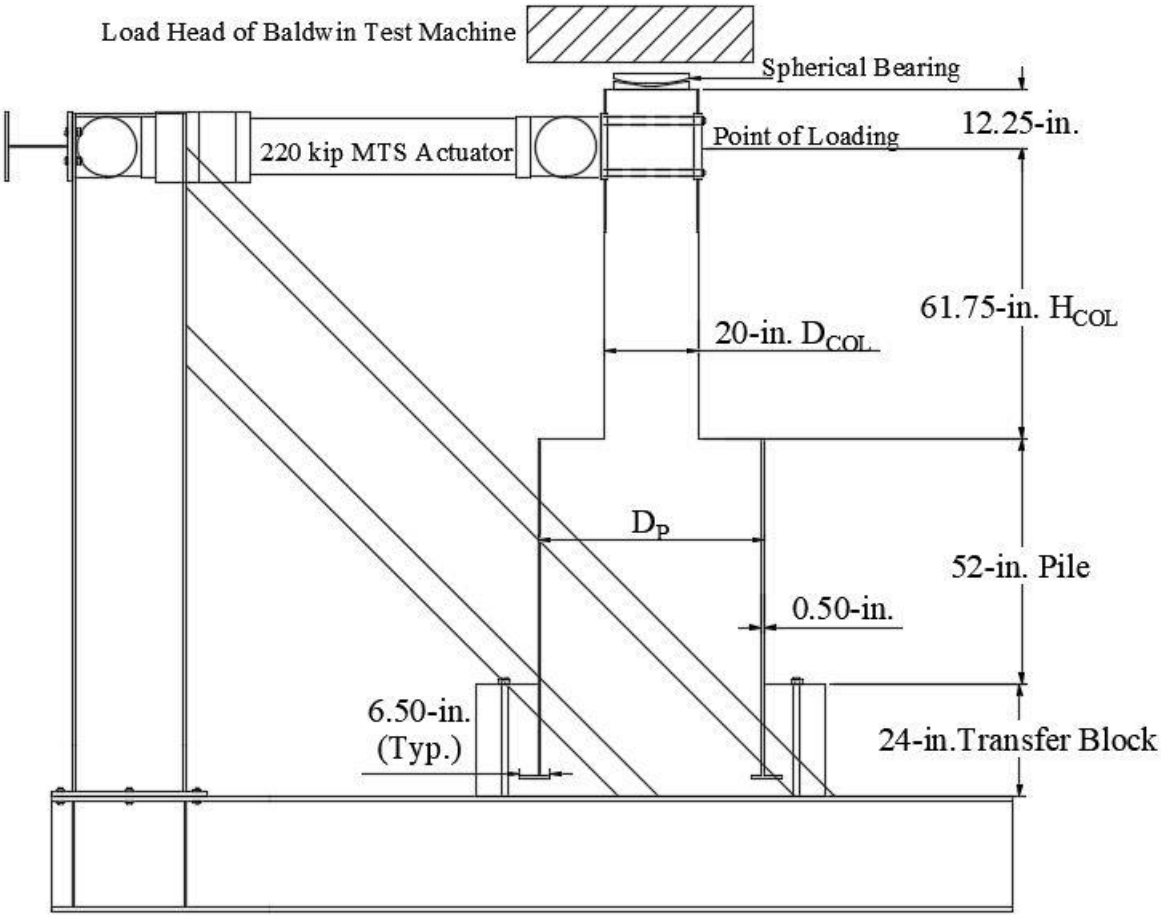

Figure 3.9. Experimental Setup Overview

The actuator was attached to the column using four 1 in high strength rods, a spreader plate, and elastomeric pads. The high-strength rods were tightened using 1 in. diameter bolts to ensure the actuator head was trndionrf to the column throughout the test. The spreader plates and rubber pads distributed the applied force over an appropriate area to prevent localized damage.

Axial loads were applied to the column using the 2400 kip Baldwin Universal testing machine. The Baldwin Universal Testing Machine applied a constant load equivalent to 7.5% of the axial capacity of the column to the top of the column, simulating loading due to superstructure and the resultant P-Δ force. Due to the different day of test concrete strengths, the axial load was not the same for both specimens. Specimen 30-21 had an axial load applied of 160 kips. Specimen 48-21 had an axial load applied of 120 kips.

To allow the top of the column to displace while having a constant axial load, an assembly was used to act as a roller support at the top of the column and is shown in Figure 3.10. The critical components of this assembly were a spherical bearing and a low friction sliding surface. The assembly included additional components to restrict out-of-plane movements and evenly transfer the vertical load from the spherical bearing to the column.

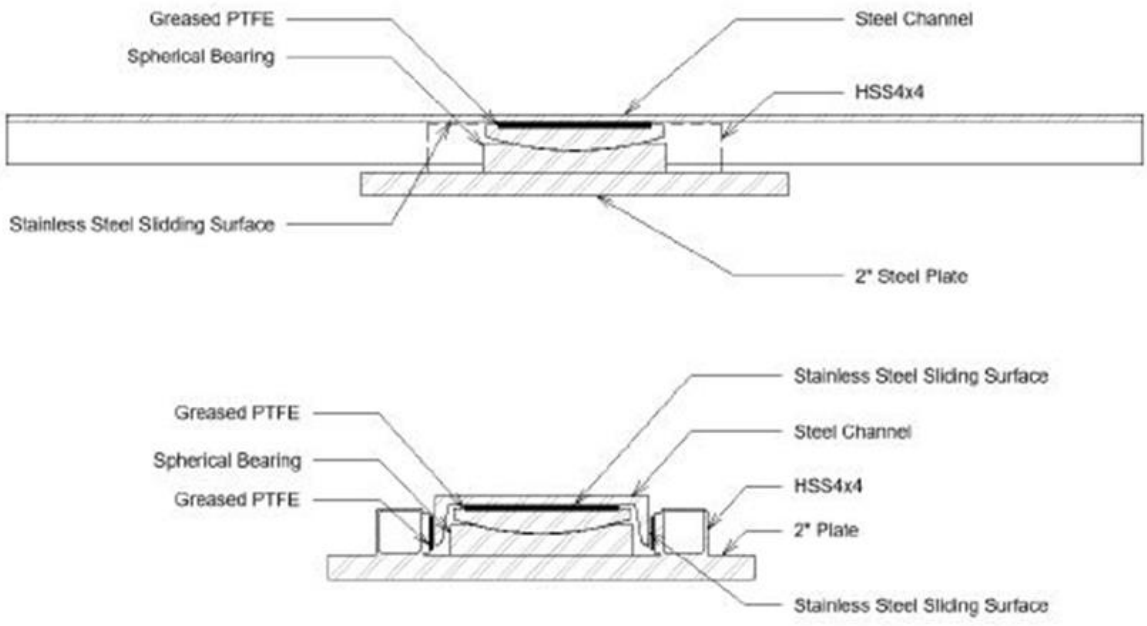

Figure 3.10. Axial Bearing Assembly for Specimen 30-21

The spherical bearing allows the top of the column to be displaced by the MTS Actuator while maintaining the Baldwin load. As shown, greased PTFE is embedded in the top of the spherical bearing. This provides a low friction sliding surface between the bearing and the channel, minimizing friction effects. The grease is a Methyl Siloxane lubricant. The bottom 2 in. thick steel plate applies the axial force from the Baldwin evenly across the top of the column. The plate also has a track for the above channel made from a HSS and more greased PTFE, as shown in Figure 3.10, to prevent transverse displacement during testing.

The large steel channel is bolted to the head of the Baldwin and acts as the top track to prevent transverse displacement. The interior web of the channel and outside flanges are lined with stainless steel providing a smooth surface on which the greased PTFE slides. A modification was made to this assembly after completion of Speciment 20-30 and this modification illustrated in Figure 3.12.

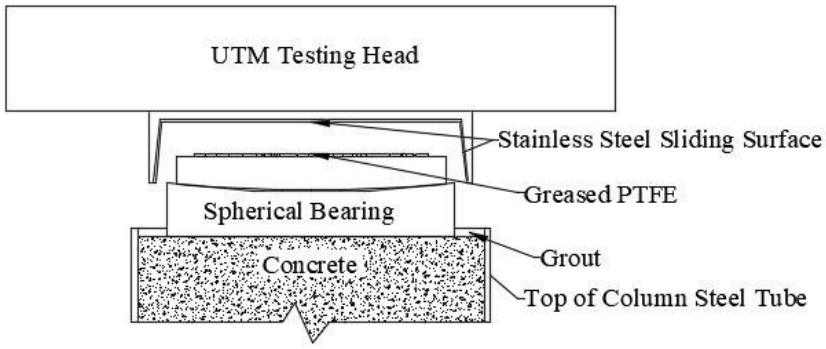

Figure 3.11. Axial Bearing Assembly

3.4 INSTRUMENTATION

To characterize the response of test specimens to lateral loading, displacements, lateral load resistance, local displacements, curvature, and strains were recorded. The imposed displacements and lateral load response were used together to characterize and compare each specimen's force drift response. The general instrument layout is shown in Figure 3.13.

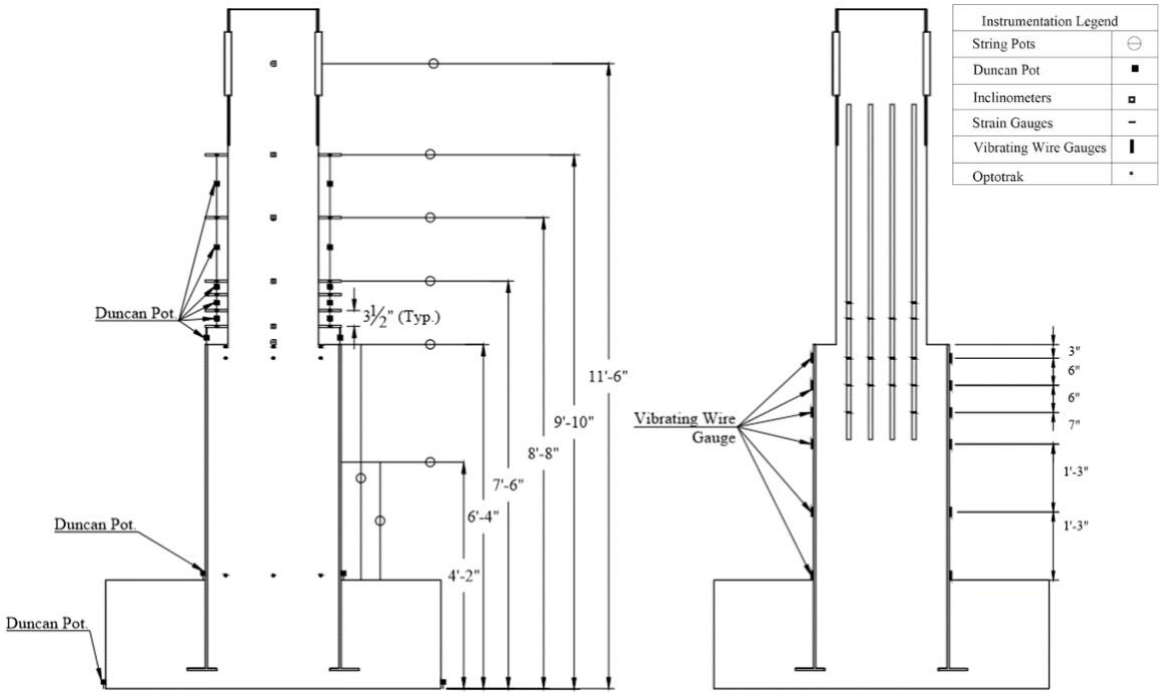

Figure 3.12. General Instrumentation Layout

Lateral and axial loads were recorded using the load cells in the MTS Actuator and the Baldwin Universal Testing machine. All exposed in the RC column and CFS pile were monitored and marked during testing. The concrete surfaces were painted white to more easily see small crack. A horizontal and vertical grid with 5 in. divisions was drawn on the column to provide location of cracking. During the test, red and blue markers were used to mark cracks, red for when the column was in compression and blue for when the column was in tension.

Displacements at the level of lateral load application and displacements along the height of the column and pile were measured to determine the deformations of the specimens under lateral loading. Displacement at the point of lateral loading was used to develop the force-displacement and moment-drift response of the various connections. This response is used to compare the performance of connections and identify how the different connections perform under lateral loads.

To monitor the displacement at the level of lateral force application and the height of the column, a reference tower was placed to the north of the specimen and multiple string potentiometers were attached between the tower and the specimen. Though the MTS Actuator LVDT was measuring displacements, these displacements were not used due to the deformation of the setup.

An Optotrak system was used to capture displacement information for the pile and column as a backup. Optotrak targets were placed along the height of the column and pile, matching some of the points where the reference column string potentiometers were attached.

Strain gauges (TML YFLA (post-yield) strain gauges) were placed on a portion of flexural reinforcement inside the column. The strain gauge readings would be used to characterize the yield behavior and compare the results from various tests. To characterize the extent of yielding in longitudinal reinforcement across the height of the test specimens, a greater number of gauges were placed on reinforcement on the most northern and southern reinforcement through the column, while fewer gauges were placed on reinforcement on the northeast and southeast reinforcement.

The strain on the outside of the pile or tube was also monitored. This was done by placing both strain gauges (TML FLA (elastic) strain gauges) and Vibrating Wire Gauges (VWGs) along the height of the pile on the northern and southern faces. The locations of these gauges were at the same height on the pile but slightly offset to the left or right of each other. VWGs were used due to the higher resolution of strain the VWG can detect compared to the regular strain gauges. The data acquisition system, used in conjunction with the gauge is more complex and is different for the VWGs than for the TML strain gauges.

To monitor the curvature of the column, inclinometers and Duncan potentiometers were used. The inclinometers, that measure the rotation of the column, were placed along the height of the column at the same heights that the string pots were attached to. At similar locations, rods going through the column were placed along its height. In between each set of rods, a Duncan potentiometer was placed to measure the deformation of the column between the rods. For the bottom rod, the rod extended out to the edge of the pile, where a Duncan potentiometer was attached and measured the difference between the rod and the top of the pile. Duncan potentiometers were also added at the base of the pile to measure any slip or uplift that the tube might experience. They were used to measure any global uplift or slipping that might have occurred during testing. Additionally, a string potentiometer was placed on a reference tower to measure the lateral actuator's push back on the testing frame.

3.5 TEST PROTOCOL

After the specimen was placed into the test rig, the instrumentation was installed. At the start of the test, the instrumentation is initialized, and axial load is applied. Then several small lateral displacement cycles are applied to verify the operation of the instrumentation. The test then proceeds under a lateral displacement control with cycles of increasing amplitude as recommended by the Applied Technology Council ATC-24.

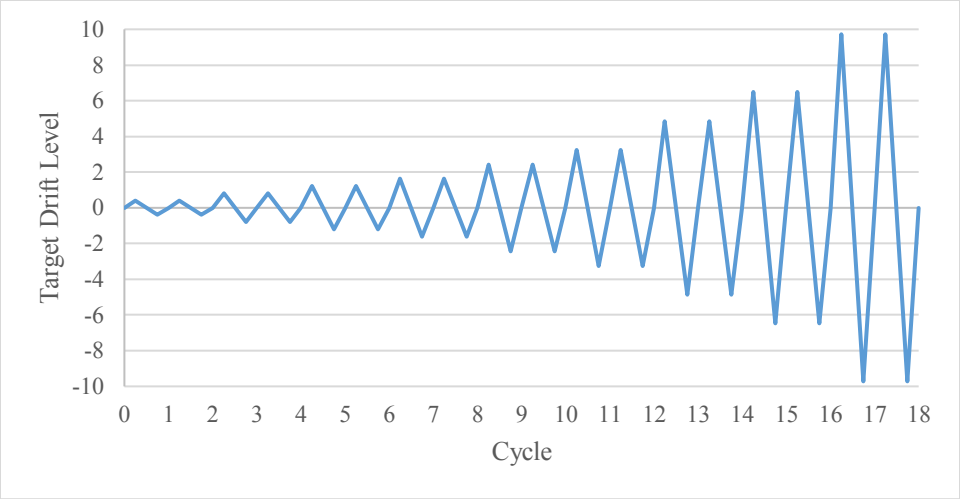

Figure 3.13. Target Displacement History

Chapter 4. EXPERIMENTAL OBSERVATIONS AND RESULTS

4.1 INTRODUCTION

Experimental testing was conducted to assess the effects of pile diameter, reinforcement embedment depth, the addition of an embedded rib inside the pile, and displacement history on the cyclic, nonlinear performance CFST pile and RC column connections specimens. Each of the four specimens was tested using the test setup and target displacement history described in the last chapter to evaluate these parameters.

Table 4.1. Specimen Test Matrix

Specimen Name	Tube Diameter (in.) [mm]	Tube Diameter/ Tube Thickness	Reinforcement Bar Size	Embedment Depth (in.) [mm]
30-21*	30 [762]	60	#7	21 [533]
48-21	48 [1219]	96	#7	21 [533]

*Specimen 30-21 is reference specimen

4.2 SPECIMEN 30-21

Specimen 30-21 was tested on February 11th, 2021 in the Structural Research Laboratory at the University of Washington. The test was performed 111 days after casting the transfer block and pile and 87 days after casting the column. The extended time between the specimen casts and testing was due to covid restrictions. The maximum measured resistances and corresponding imposed drift of each cycle are provided in Table 4.2. The force-drift and moment-drift hysteresis curves of the column are shown in Figures 4.1-4.4. The constant axial load applied to this specimen was 7.5% of the axial capacity of the column, 160 kips.

Table 4.2. Maximum Resistances and Drifts in Each Cycle (30-21)

Target Drift	Cycle	Maximum Measured Resistance (kips)		Maximum Imposed Drift (%)	
		Tension	Compression	Tension	Compression
1.62%	1	77.93	63.14	1.11	1.06
	2	58.34	63.75	0.96	0.92
	3	65.54	63.14	0.94	0.93
2.43%	4	80.02	72.31	1.52	1.52
	5	81.07	77.13	1.55	1.54
3.23%	6	89.20	78.13	2.19	2.23
	7	86.89	74.84	2.25	2.30
4.86%	8	95.13	79.36	3.65	3.77
	9	85.09	80.38	3.71	3.82
6.48%	10	91.89	83.27	5.03	4.95
	11	86.28	78.30	5.13	4.98
9.72%	12	85.61	77.74	7.03	6.59
	13	48.61	18.16	7.51	8.06

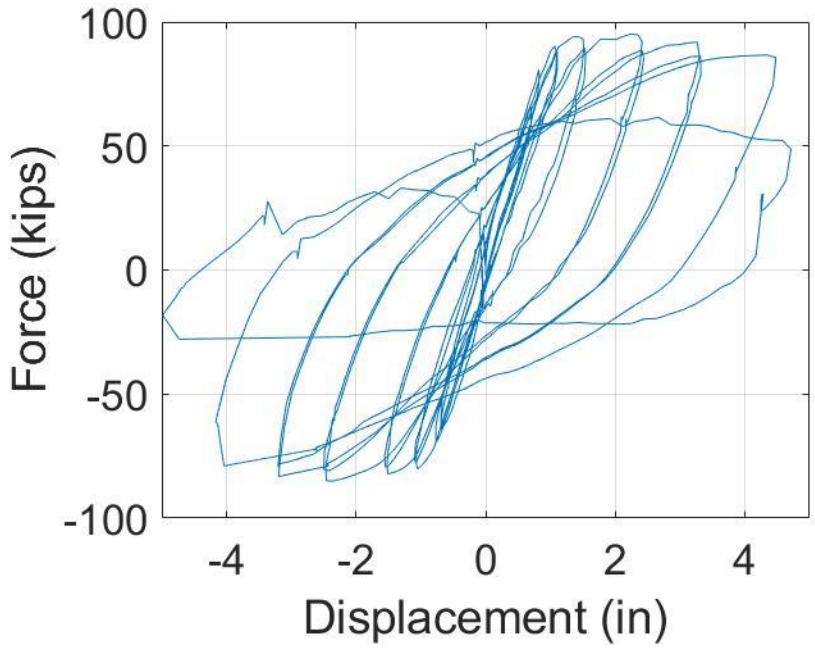

Figure 4.1. Specimen 30-21 Force-Displacement Curve

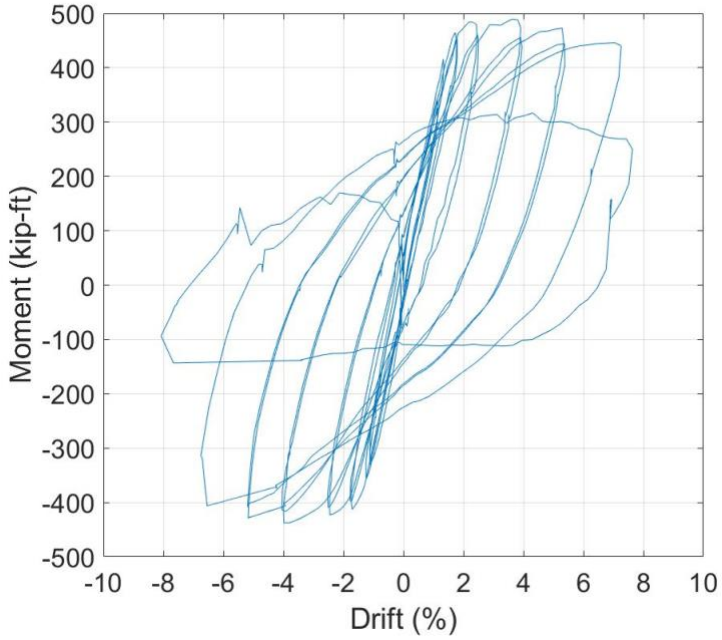

Figure 4.2. Specimen 30-21 Moment-Drift Curve with P-Δ Effects Removed

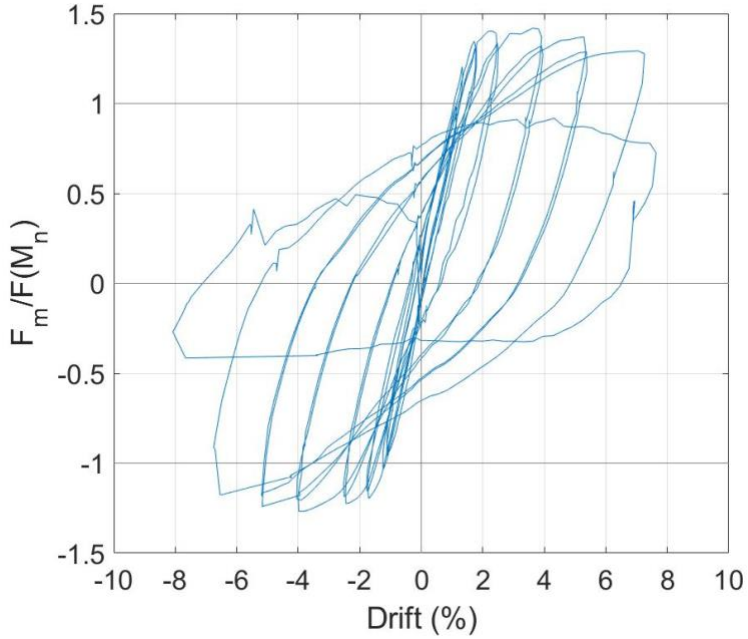

Figure 4.3. Specimen 30-21 Normalized by F_n Force-Drift Curve with P-Δ Effects Removed

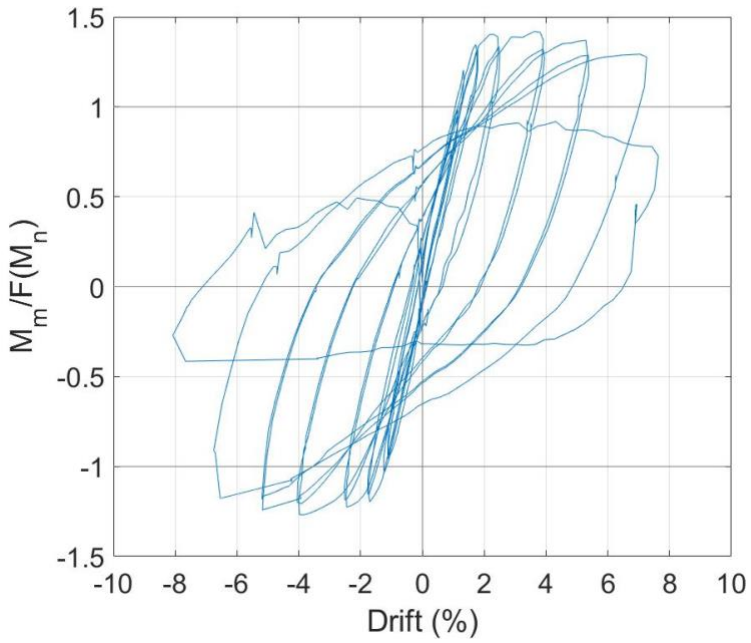

Figure 4.4. Specimen 30-21 Normalized by M_n Moment-Drift Curve with P-Δ Effects Removed

As shown in Table 4.1 and Figures 4.1 - 4.4, the largest moment, M_p, and corresponding drift reached by this specimen were 489.5 kip-ft or 1.42 M_n, at 3.7% drift. The nominal moment, M_n, for Specimen 30-21 was 345.1 kip-ft. The strength degraded approximately 6% of M_p or 30 kip-ft with each of the following cycles at 5.0% and 7.3% drifts, and then substantially drops 40% of M_p or 190 kip-ft with the last cycle, which reached the largest drift of 7.5%. The behavior is similar on the negative drift side as well.

As mentioned previously, the dry run for this Specimen had a displacement of 1 in. instead of the planned 0.1 in. This caused the column and the column reinforcement to yield and to enter the inelastic region before originally planned. Due to this, displacements less than 1 in. were skipped for this specimen's displacement history. The results of the dry run were appended to the beginning of the test results.

Table 4.3 shows the width and location of the maximum and residual cracks measured for each drift level.

Table 4.3. Maximum Measured Crack Widths and Locations for Each Drift Level (30-21)

Drift Level	Maximum Crack		Residual Cracks	
	Width (mm)	Location	Width (mm)	Location
1.0%	0.5	Base of Column	0.1	11 in. above base
1.5%	1.0	Base of Column	0.3	5 in. above base
2.2%	2.0	Base of Column	0.9	5 in. above base
3.7%	3.0	Base of Column	1.0	11 in. above base
5.0%	3.0	Base of Column	2.0	5 in. above base
7.0+%	3.5	Base of Column	3.0	10 in. above base

4.2.1 Low Drift Cycles (0-2.0% Drift)

At approximately 1.1% drift, the lateral force ranged from -0.9 to 1.2 times the nominal force, $F_{n,}$ of 67.1 kips (-63.1 to 77.9 kips) as shown in Figure 4.1.

Small horizontal cracks, less than 0.5 mm in width, formed along the height of the column during this cycle, primarily on the northern and southern faces of the column, as shown in Figure 4.5.

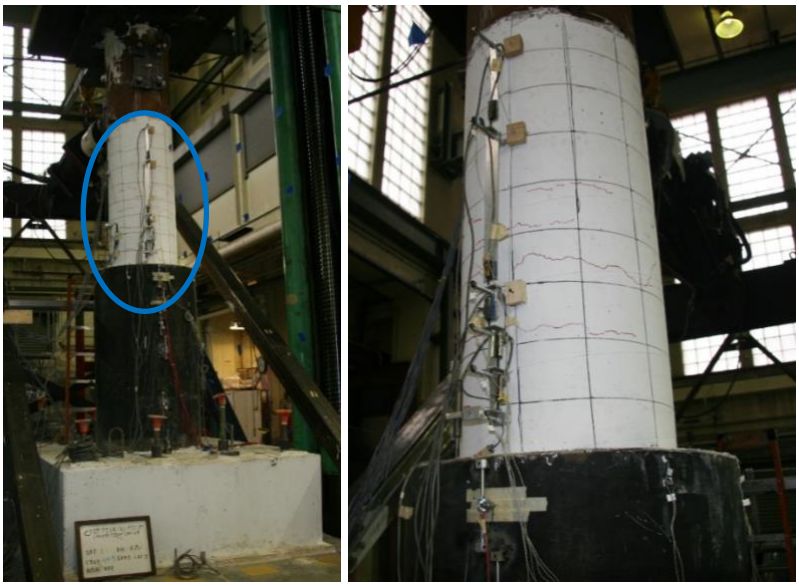

Figure 4.5. Specimen 30-21 Horizontal Cracks on North Column Face

During this cycle, the Northeast (NE), Southeast (SE), and Southern (S) longitudinal reinforcing bars in the column exceeded the reinforcement yield strain of 0.0024 in/in, from $0.45D_{COL}$ to $-0.45D_{COL}$. Gauges below this range are in the elastic range. As shown in Figure 4.6, the reinforcement has yielded at multiple locations but had not yielded at $-0.75\ D_{COL}$.

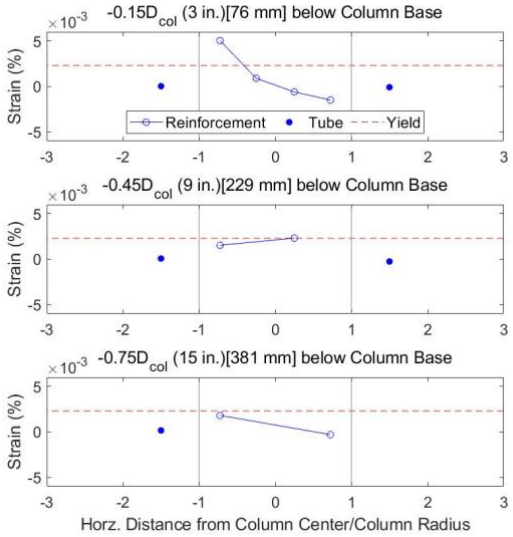

Figure 4.6. Specimen 30-21 Strain Distribution at 1.1% Drift

The next cycle was to 0.9% drift and was the first cycle during the actual testing and thus has a slightly smaller drift level than the previous cycle. At 0.9% drift, the lateral load had a range of -1.0 to $0.98F_n$ (-63.75 to 65.5 kips), which was a decrease of $0.1F_n$ from the previous cycle, shown in the figures.

Horizontal cracks formed along the height of the column on both the north and south sides. The cracks, at the interface of the column and the top of the pile, ranged in width from 0.3mm to 0.5mm, shown in Figure 4.7.

Figure 4.7. Specimen 30-21 Interface Cracks on Southern Face at 0.9% Drift

The reinforcement at the peak of these cycles registered strains greater than yield in all the Northern (N), NE, and S bars, at locations -0.15D_{COL}, 0.30D_{COL}, and 0.45D_{COL} when the column was in tension. When the column was cycled in compression, no reinforcement strains measured were greater than the yield strain.

At 1.5% drift, the lateral load ranged from -1.1 to 1.21F_n (-77.1 to 81.1 kips), an increase of 0.2F_n from the previous cycle.

Radial cracks formed at three different locations on the top of the pile, going from the perimeter of the pile to the column, shown in Figure 4.8.

Figure 4.8. Specimen 30-21 Radial Cracks on North Face of Column

On the second cycle to 1.5% drift, diagonal cracks started to form $1.8D_{COL}$ (36 in.) above the base of the column, and the existing horizontal crack widths increased, with the largest width reaching 1 mm. During these cycles, when the column was in compression, all the strain gauge locations, except for $-0.75D_{COL}$ on the northern (N) bar reinforcement measured a strain greater than yield, Figure 4.9. The same was true for the southern (S) bar reinforcement when the column was in tension.

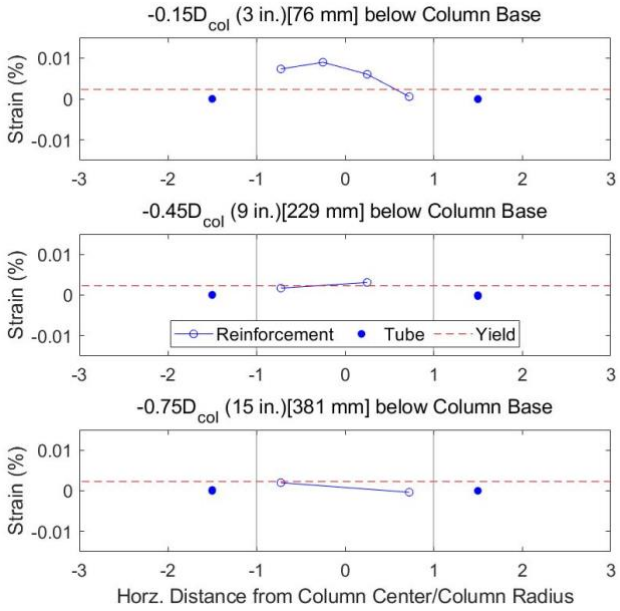

Figure 4.9. Specimen 30-21 Strain Distribution at 1.5% Drift

4.2.2 Moderate Drift Cycles (2.0-4.0% Drift)

At a drift of 2.2%, the lateral loads ranged from -1.2 to $1.3F_n$ (-78.1 to 89.2 kips), an increase of $0.1F_n$ from the previous cycle.

Spalling occurred at the bottom 2.5 in. of the column, but no reinforcing bars were exposed. The horizontal cracks increased to a maximum width of 2 mm, shown in Figure 4.10, with the largest cracks being at the interface of the column and the top of the pile, with the largest crack width being 1.75 mm.

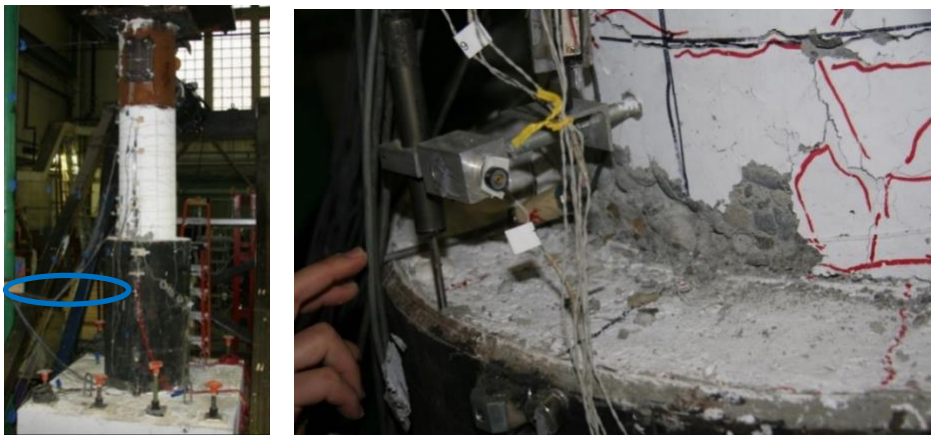

Figure 4.10. Specimen 30-21 Initial Spalled Region on North Face at 2.2% Drift

At these peak drift levels, the reinforcement strain measured at the -0.75D_{COL} location stayed right at or below the yield strain. The rest of the measured strain locations (-0.30D_{COL}, -0.15 D_{COL}, 0.30D_{COL}, and 0.45D_{COL}) were well above the yield strain, reaching strains up to 0.016 in./in. when that side sustained tension, shown in Figure 4.11.

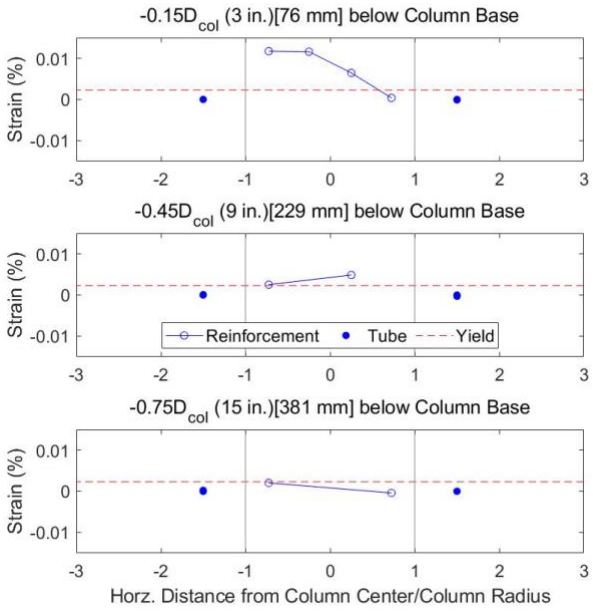

Figure 4.11. Specimen 30-21 Strain Distribution at 2.2% drift

At drift cycles of approximately 3.7%, the lateral loads ranged from -1.2 to 1.42F_n (-80.4 to 95.1 kips), approximately equal to the previous cycle. The 1.42F_n (95.1 kips) lateral load was

the maximum lateral load the column experienced during this test. This occurred during the first cycle at this drift level.

The crack widths at the column base continued to increase to a maximum width of 3 mm. The spalling increased to the point where transverse reinforcement, #3 hoops located approximately 3 in. from the base of the column, was exposed on the second cycle, shown in Figure 4.12.

Figure 4.12. Specimen 30-21 Spalled Region on Northern Column Face at 3.7% Drift

The stains measured at the peaks of this cycle all exceeded the yield strain, except for the S bar location at -0.75 D_{COL} as shown in Figure 13.

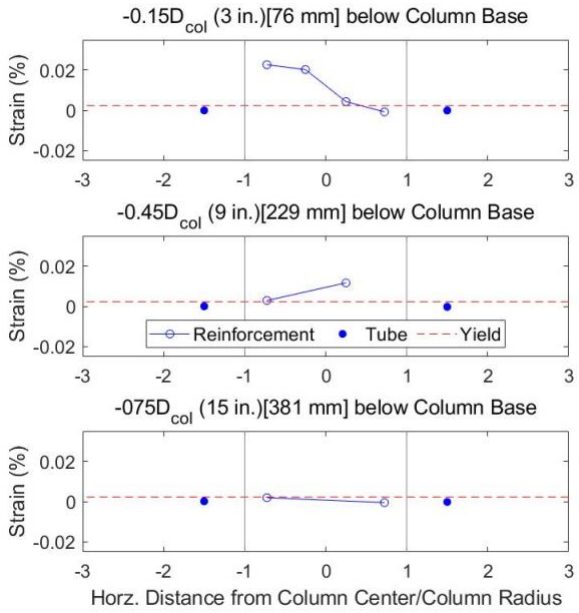

Figure 4.13. Specimen 30-21 Strain Distribution at 3.7% drift

4.2.3 Large Drift Cycles (Greater than 4.0% Drift)

At drift cycles of 5%, the lateral loads ranged from -1.2 to 1.37F_n (-83.3 to 91.9 kips), a decrease of approximately 0.05F_n from the previous cycle.

The spalled region increased to 0.50D_{COL} (10 in.) above the base of the column and multiple transverse reinforcement bars and the first longitudinal reinforcement were exposed on the northern face of the column, shown in Figure 4.14. There was a 3 mm wide crack at the interface of the column and the top of the pile.

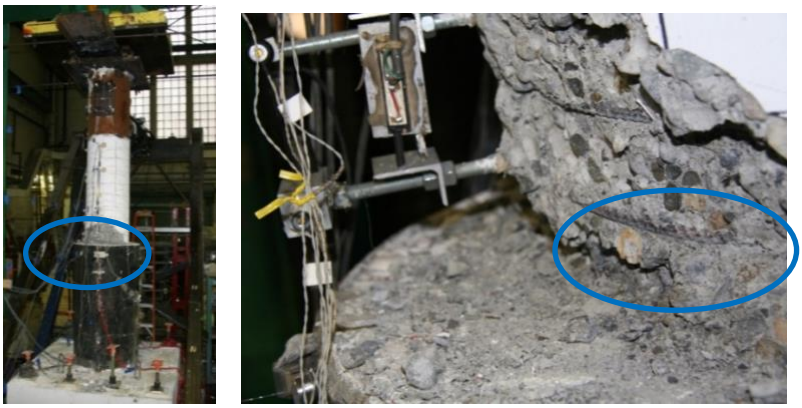

Figure 4.14. Specimen 30-21 Exposed Longitudinal Reinforcement on South Face

As with the previous cycles at 3.7% drift, all the reinforcement strains measured were above the yield strain except for the S bar's -0.75D_{COL} location, which is shown in Figure 4.15.

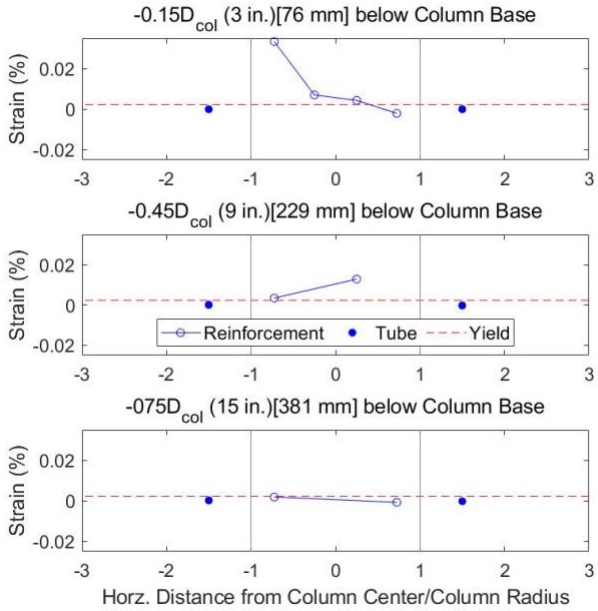

Figure 4.15. Specimen 30-21 Strain Distribution at 5% Drift

For this cycle at 5% drift and the remaining cycles that had equal or larger drifts, the axial binding issue of the bearing mentioned in Chapter 3 occurred. This was seen when plotting the original hysteretic force-displacement curve of the test. There were spikes in the measured lateral resistance due to this binding of the axial bearing assembly for the negative drift. These spikes in lateral force were removed from the data and true lateral resistances replaced were determined by examination of the data prior to binding and the data from the opposite direction of loading which did not make binding contact. Figures 4.16-4.17 are a comparison of the moment-drift hysteresis curves before and after the lateral resistance corrections. As noted in prior discussion the bearing assembly was modified to avoid the binding at large rotations in future tests.

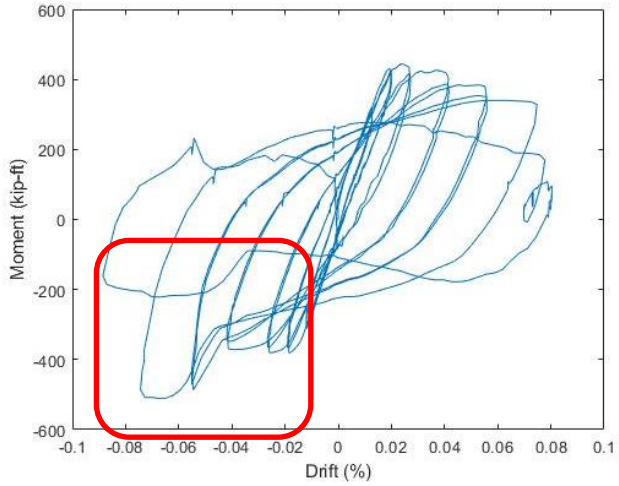

Figure 4.16. Specimen 30-21 Original Moment-Drift Curve

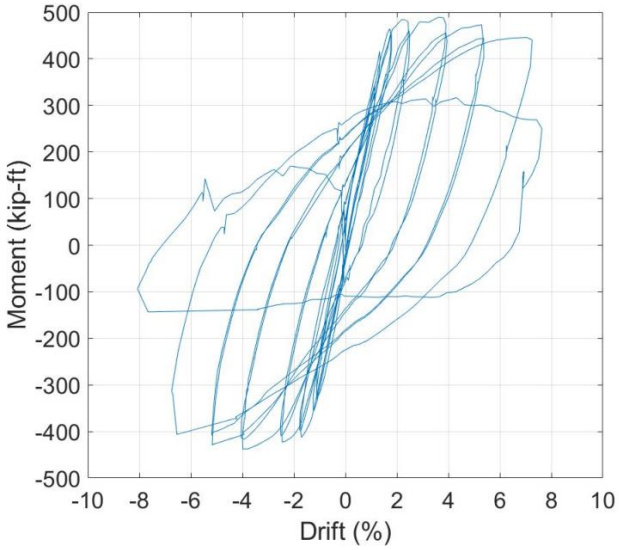

Figure 4.17. Specimen 30-21 Corrected Moment-Drift Curve

At 7.3% drift, the lateral loads ranged from -1.2 to 1.3F_n (-77.7 to 85.6 kips), a decrease of 0.1F_n from the previous cycle.

The spalled region reached 0.875 D_{COL} (17.5 in.) on both the North and South sides. There was a 3+ mm wide crack at the base of the column. This crack was due to pullout failure of the reinforcing bars. This extensive spalled region and interface cracks are shown in Figure 4.18.

a) b)

Figure 4.18. Specimen 30-21 a) Major Spalled Region on Southern Column Face, b) Large Crack at Northern Column Interface at 7.3 % Drift

Loading was terminated after the second cycle at 8% drift when the longitudinal reinforcement bars had buckled when the column was both in tension and compression. The lateral load during this cycle reached a peak of $0.72F_n$ (48.6 kips), a $0.7F_n$ reduction in resistance from the peak force. During this second cycle, the transverse reinforcement and concrete seemed to explode or pop out. Two of the transverse reinforcement hoops, at 4 in and 7 in from the base of the column, their ends, which had 90-degree hooks, opened. This happened as the column was cycled in both tension and compression. After the second cycle, the concrete at the base of the column had completely crushed, and there was no continuous concrete going from the base of the column above $0.15D_{COL}$ (3 in.) to the rest of the column. The final state of the column is shown in Figure 4.19.

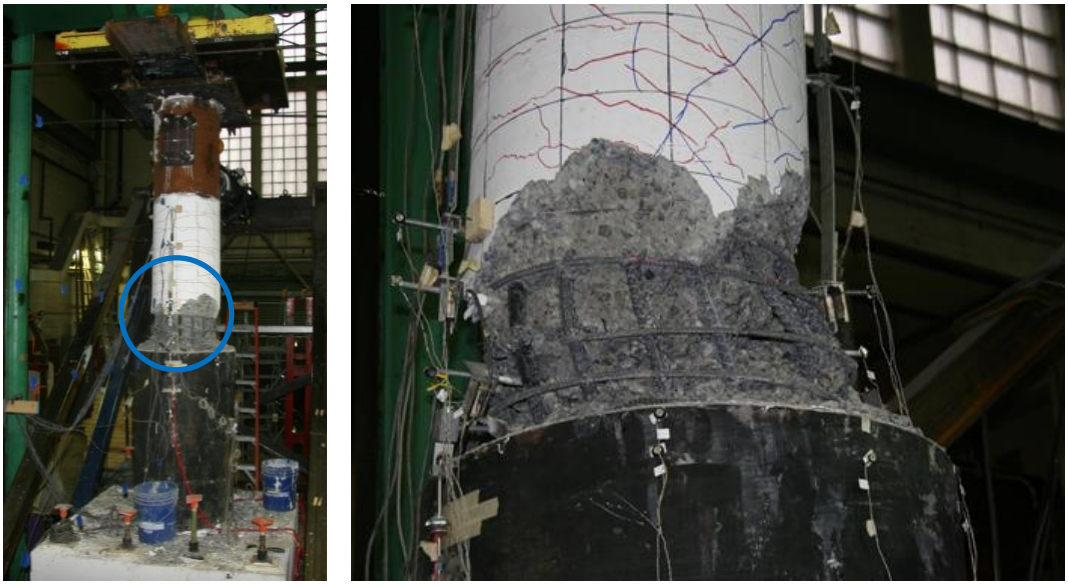

Figure 4.19. Specimen 30-21: Failed Specimen 30-21 at 8% Drift

Throughout all load cycles, the pile and transfer block showed no visible damage. There was no buckling or yielding of the pile. The largest measured tube strain was 0.0006 in/in, which occurred at 52 in. below the top of the tube, during the 3.7% drift cycles. There was no noticeable slip between the pile concrete in comparison to the edge of the steel tube at any point of the test. No cracks formed anywhere on the transfer block. After the test was finished, the column was removed from the top of the pile. As shown in Figure 4.20, except for the radial cracks and minor concrete damage around the base of the column, the top of the pile concrete appears to be largely undamaged.

Figure 4.20. Top of Specimen 30-21 Pile with Column Removed

4.3 SPECIMEN 48-21

Specimen 48-21 was tested on March 11th, 2021 in the Structural Research laboratory at the University of Washington. The test was performed 39 days after casting the transfer block, 32 days after casting the pile, and 10 days after casting the column. The column concrete had met the required design strength and was ready to be tested.

As stated before, Specimen 48-21 was identical to Specimen 30-21, except for the tube diameter, which was 48 in. instead of 30 in. An elastic cycle at 0.1 in. displacement was run on this specimen, as the dry run for the test. The maximum measured resistances and corresponding imposed drifts of each cycle are provided in Table 4.4. The force-displacement and moment-drift hysteresis curves of the column are shown in Figures 4.21 – 4.24. The constant axial load applied to this specimen was 7.5% of the axial capacity of the column, 120 kips.

Table 4.4. Maximum Resistances and Drifts in Each Cycle (48-21)

Target Drift	Cycle	Maximum Measured Resistance (kips)		Maximum Imposed Drift (%)	
		Tension	Compression	Tension	Compression
0.40%	1	32.6	30.8	0.20	0.12
	2	31.5	29.1	0.20	0.19
0.81%	3	54.0	49.9	0.49	0.48
	4	52.7	46.7	0.50	0.49
1.21%	5	67.4	62.6	0.75	0.76
	6	62.7	62.0	0.76	0.75
1.62%	7	74.0	73.7	1.11	1.10
	8	68.3	65.5	1.14	1.15
2.42%	9	81.9	80.5	1.82	1.82
	10	81.1	77.1	1.84	1.84
3.24%	11	82.2	83.8	2.62	2.57
	12	82.5	78.1	2.64	2.62
4.86%	13	84.8	8.6	4.22	4.10
	14	NA	79.1	NA	4.11
6.48%	15	84.7	84.8	5.91	5.65
	16	78.9	72.6	5.95	5.69
9.72%	17	37.1	37.1	9.52	8.53
	18	12.7	32.8	9.66	8.98

Due to operating error, the tension peak for cycle 14 was missed. When finishing the compression peak hold, the “Return to Zero” displacement button was accidentally hit which caused the cycle to end and the tension peak to be skipped.

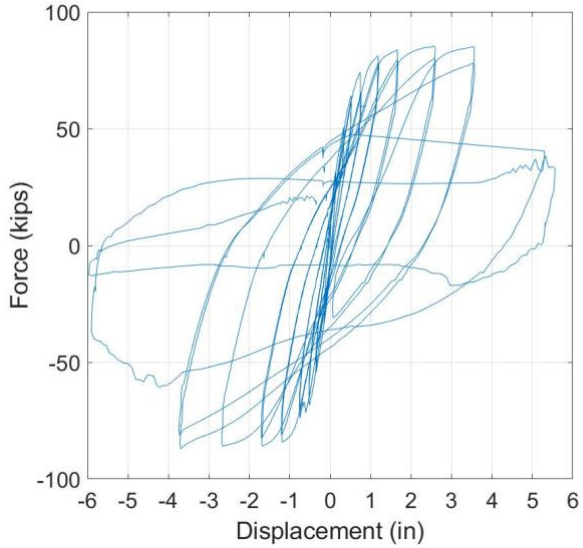

Figure 4.21. Specimen 48-21 Force-Displacement Curve

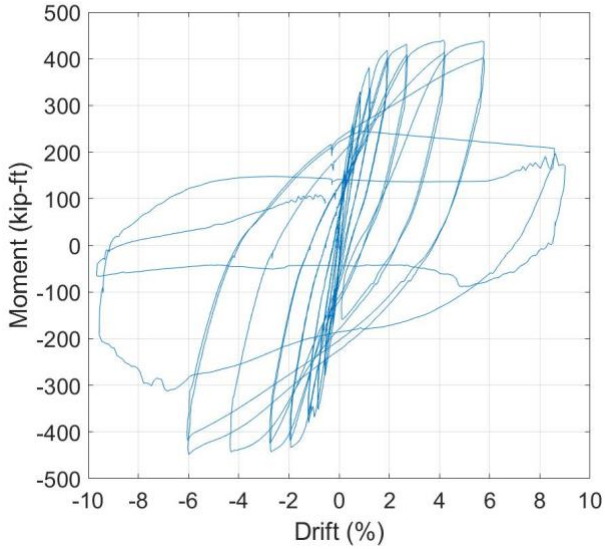

Figure 4.22. Specimen 48-21 Moment-Drift Curve with P-Δ Effects Removed

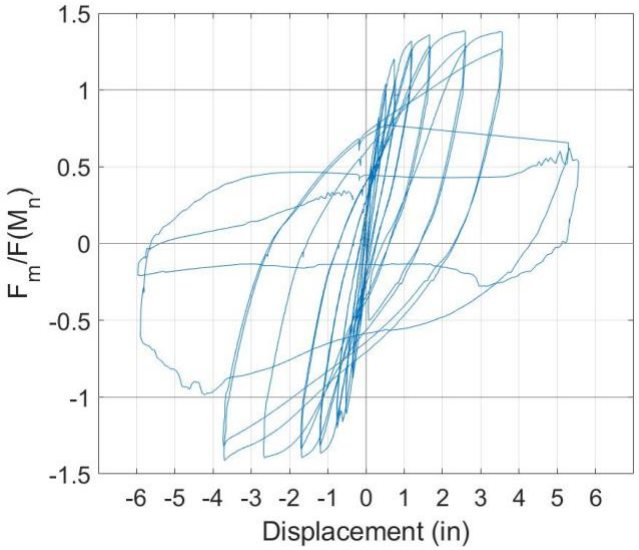

Figure 4.23. Specimen 48-21 Force-Displacement Curve with P-Δ Effects Removed Normalized by F_n

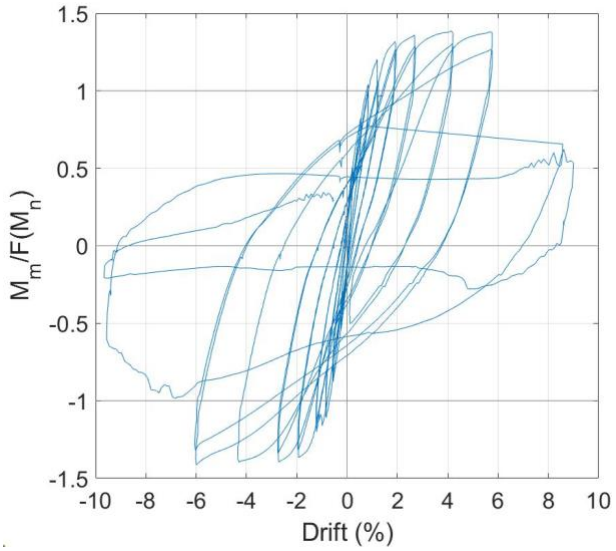

Figure 4.24. Specimen 48-21 Moment-Drift Curve with P-Δ Effects Removed Normalized by M_n

As shown in Table 4.4 and Figures 4.21-4.24, the largest moment, M_p, and corresponding drift reached by this specimen were 436.5 kip-ft or 1.38 M_n, at 5.5% drift. The nominal moment, M_n, was 317.3 kip-ft for Specimen 48-21. The lateral strength increased approximately 2% of M_p, or 10 kip-ft for each of the previous cycles at 2.6% and 4.1% drifts, and then substantially drops

46% of M_p or 200 kip-ft with the last two cycles, which reached the largest drift of 9.7%. The behavior is similar on the negative drift side as well. The largest moment, 436.5 kip-ft, does line up with the largest lateral resistance, 84.8 kips, when accounting for P-Δ delta effects.

Table 4.5 shows the width and location of the maximum and residual cracks measured for each drift level.

Table 4.5. Maximum Measured Crack Widths and Locations for Each Drift Level (48-21)

Drift Level	Maximum Crack		Residual Cracks	
	Width (mm)	Location	Width (mm)	Location
0.2%	0.2	9 in. above base	NA	NA
0.5%	0.5	Base of Column	0.1	Base of Column
0.8%	0.8	Radial top of Pile	<0.1	Base of Column
1.1%	1.5	Base of Column	0.1	Base of Column
1.8%	2.5	Base of Column	0.6	Base of Column
2.6%	3.5	Base of Column	0.5	Base of Column
4.2%	4.0	Base of Column	2.0	7 in. above base
6.0%	3.5	9 in. above base	Spall	Base of Column
9.0+%	Spall	Base of Column	Spall	Base of Column

4.3.1 Low Drift Cycles (0-2.0% Drift)

For drift cycles of approximately 0.2% and 0.5%, the lateral loads ranged from -0.5 to 0.5 times the nominal force, F_n, of 61.7 kips (-32.6 to 30.8) kips and -0.9 to 0.8F_n (-54.0 to 49.9 kips), respectively, as shown in Figure 4.21-4.24.

Small horizontal cracks formed 21 in. up the height of the column on both the northern and southern faces of the column, shown in Figure 4.25. The largest crack had a width of 0.5 mm wide. No residual cracks were measured at zero force.

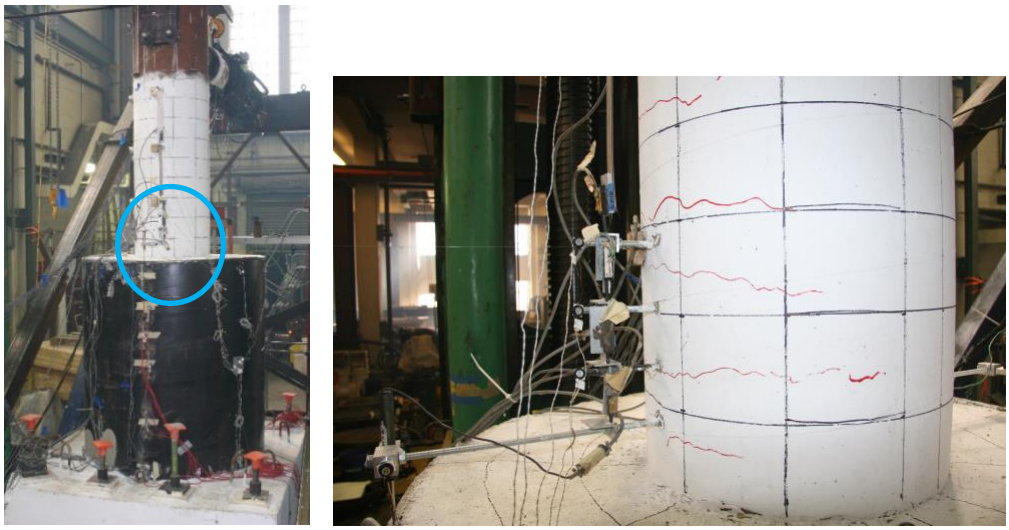

Figure 4.25. Specimen 48-21 Horizontal Cracks on North Column Face at 0.2% Drift

None of the longitudinal reinforcement strain measurements during the peak displacement exceeded the yield strain.

At 0.8% drift, the lateral load ranged from -1.1 to $1.0F_n$ (-67.4 to 62.6 kips), an increase of $0.2F_n$ from the previous cycle.

The already formed horizontal cracks continued to propagate circumferentially. The maximum width measured was 0.7 mm. New horizontal cracks formed 40 in. above the column base. Radial cracks were also measured at this displacement on the top of the pile shown in Figure 4.26. The radial cracks had a maximum width of 0.8 mm. From this point on additional radial cracks did not form and the already formed radial cracks did not expand in width.

Figure 4.26. Specimen 48-21 Radial Cracks on Top of Pile Concrete at 0.8% Drift

The column reinforcement strain exceeded the reinforcement yield strain of 0.0024 in/in at the peak displacement of this cycle. The largest strain was measured on the extreme Southern (S) bar of the column at -0.15D_{COL}.

The strain distribution plots (see Figure 4.27) for Specimen 48-21 have a similar format to Specimen 30-21. However, the S bar strain gauges at the 0.3D_{COL} and -0.45D_{COL} locations were broken before testing and no readings were able to be used from them, thus there are only 3 dots for the plot at 0.3D_{COL} and 1 dot for the -0.45D_{COL} locations plot.

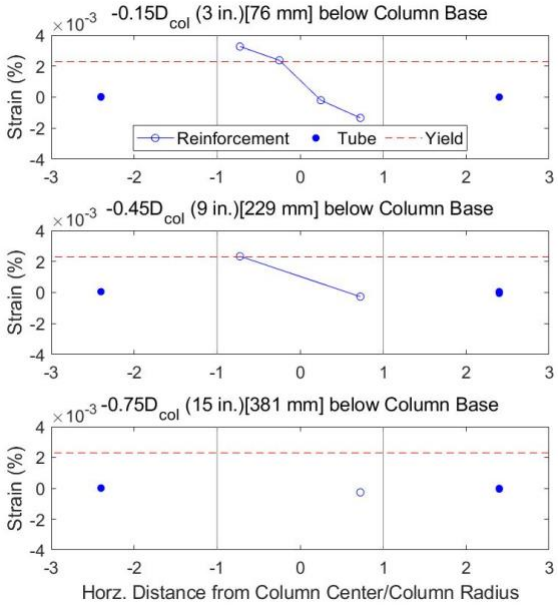

Figure 4.27. Specimen 48-21 Strain Distribution at 0.8% Drift

At drift cycles of 1.1%, the lateral load ranged from -1.2 to 1.2F_n (-74.0 to 73.7 kips), an increase of 0.15F_n.

The horizontal cracks continued to widen to a maximum width of 1.5 mm, as well as audible cracking was heard. During zero force, small residual cracks were noted, having a maximum width less than 0.1 mm, shown in Figure 4.28.

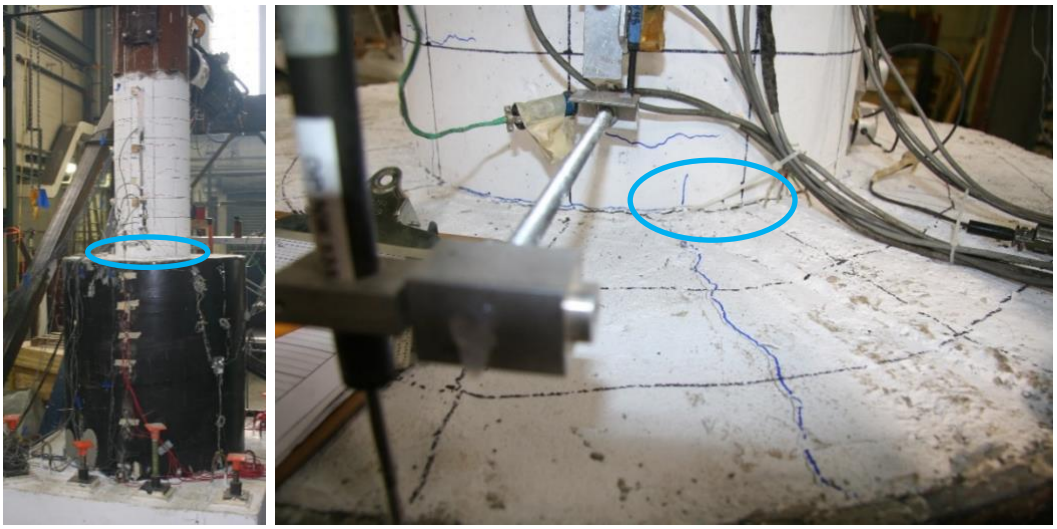

Figure 4.28. Specimen 48-21 Vertical Residual Force Crack at 1.1% Drift

The strains measured during the peak displacement of these cycles exceeded the yield strain at locations $0.3D_{COL}$, $-0.15\ D_{COL}$, $-0.3D_{COL}$, and $-0.45D_{COL}$ on both the N and S bars. The strain gauge located at $-0.75D_{COL}$ did not reach the yield shown in Figure 4.29.

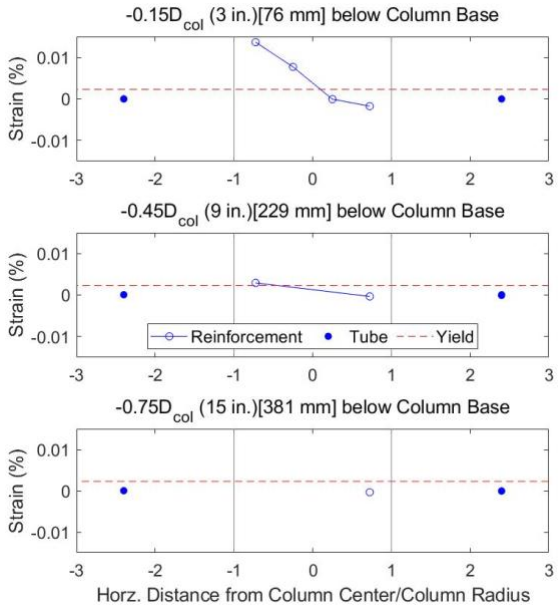

Figure 4.29. Specimen 48-21 Strain Distribution at 1.1% Drift

At drift displacements of 1.8%, the lateral load ranged from -1.3 to $1.3F_n$ (-81.9 to 80.5 kips), an increase of $0.1F_n$.

The already formed horizontal cracks expanded, with the maximum horizontal crack width measured at 2.5 mm. This crack was at the base of the southern face of the column shown in Figure 4.30.

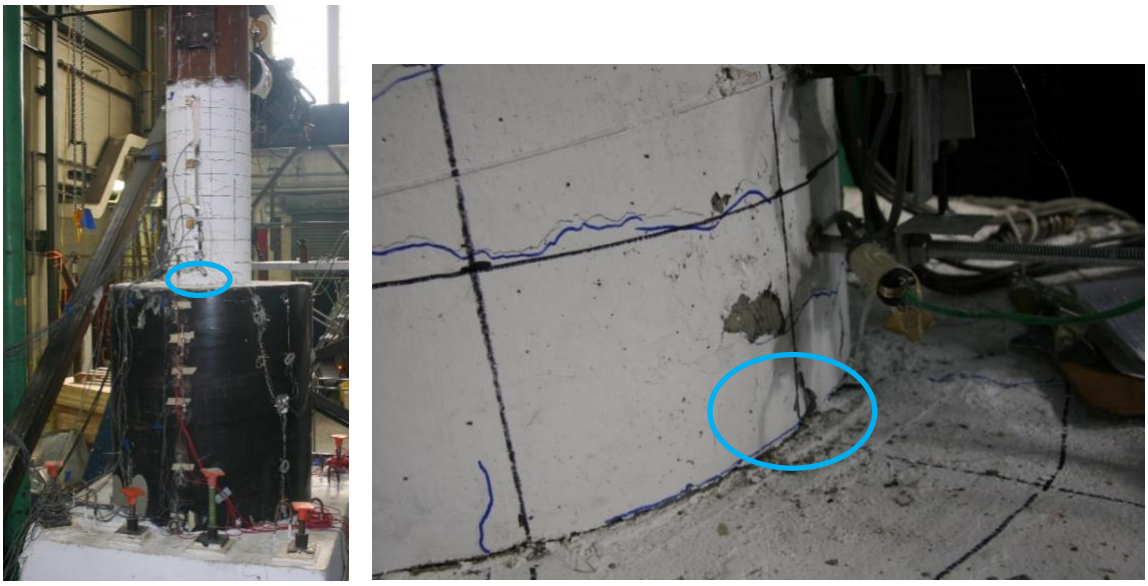

Figure 4.30. Specimen 48-21 Column Interface crack at 1.8% Drift

The strains measured at the peak displacement of these cycles all exceeded the yield of the reinforcement, with the largest strain, 0.015 in/in, occurring at -0.15D_{COL} on the S bar as shown in Figure 4.31. The -0.75D_{COL} location did not reach the yield strain.

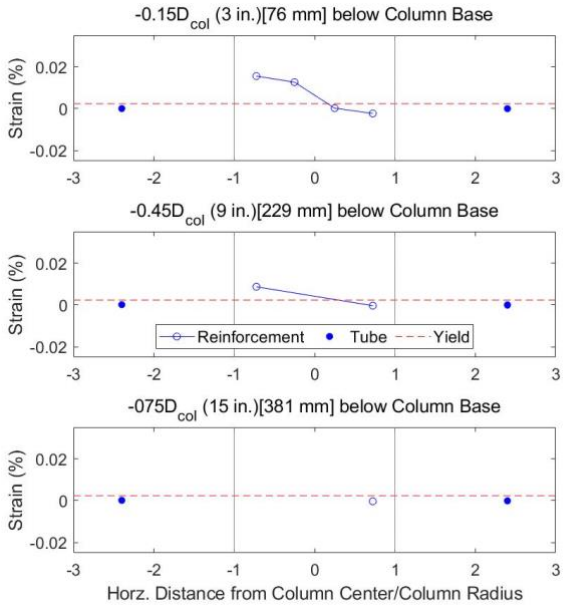

Figure 4.31. Specimen 48-21 Strain Distribution at 1.8% Drift

4.3.2 Moderate Drift Cycles (2.0-4.0% Drift)

On the following cycle, at 2.6% drift, the lateral loads ranged from -1.3 to 1.3F_n (-82.5 to 83.8 kips), approximately equivalent to the previous cycle.

The horizontal cracks continued to expand, with the widest crack occurring at the base of the southern side of the column with a width of 3.5 mm. During zero force, a 1 in. section of concrete spalled off on the northwestern face of the column. New residual cracks formed on the northern face, while the cracks on the southern face closed up. There was an increase in the spalling on both the northern and southern sides of the column continued to expand as shown in Figure 4.32.

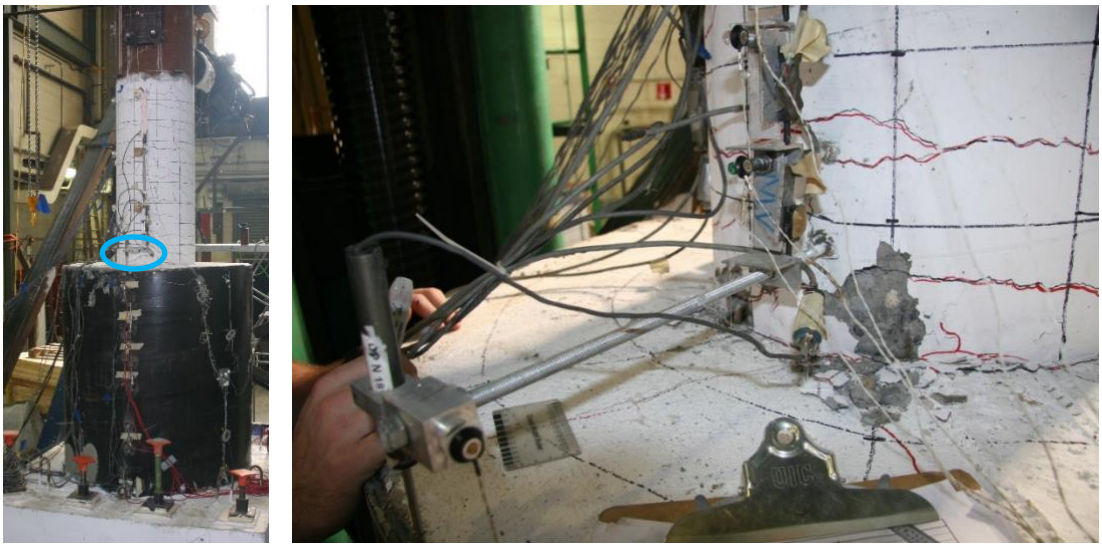

Figure 4.32. Specimen 48-21 Spalled Region at Base of North Face of Column at 2.6% Drift

The strains measured at the peak displacement of these cycles all exceeded the yield of the reinforcement, reaching a maximum strain of 0.022 in/in on the -0.15D_{COL} location on the S bar location. The -0.75D_{COL} location on the N bar did not reach the yield strain, as shown in Figure 4.33.

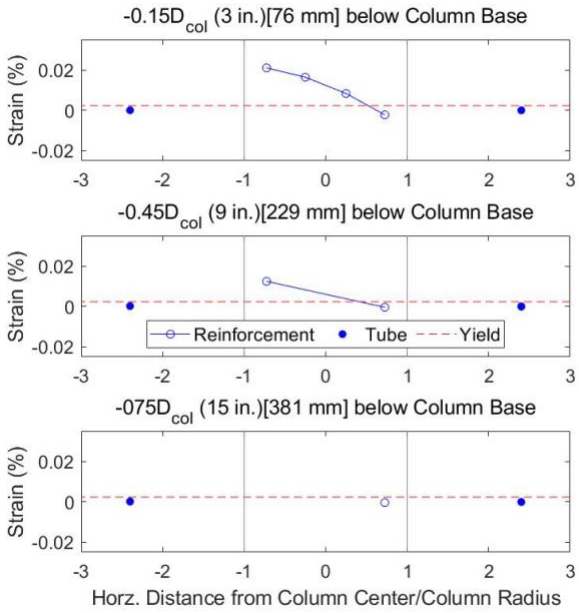

Figure 4.33. Specimen 48-21 Strain Distribution at 2.6% Drift

4.3.3 Large Drift Cycles (Greater than 4.0% Drift)

At drift cycles of 4.1%, the lateral load ranged from -1.4 to 1.4F_n (-84.8 to 84.6 kips), approximately equivalent to the last cycle.

The spalling at the northern base of the column increased to the point where the column reinforcement, both transverse and longitudinal, was exposed as shown in Figure 4.34. The crack between the base of the column and the top of the pile continued to expand to a maximum width of 4 mm. During zero force, no new residual cracks formed or spall developed, unlike the previous cycle.

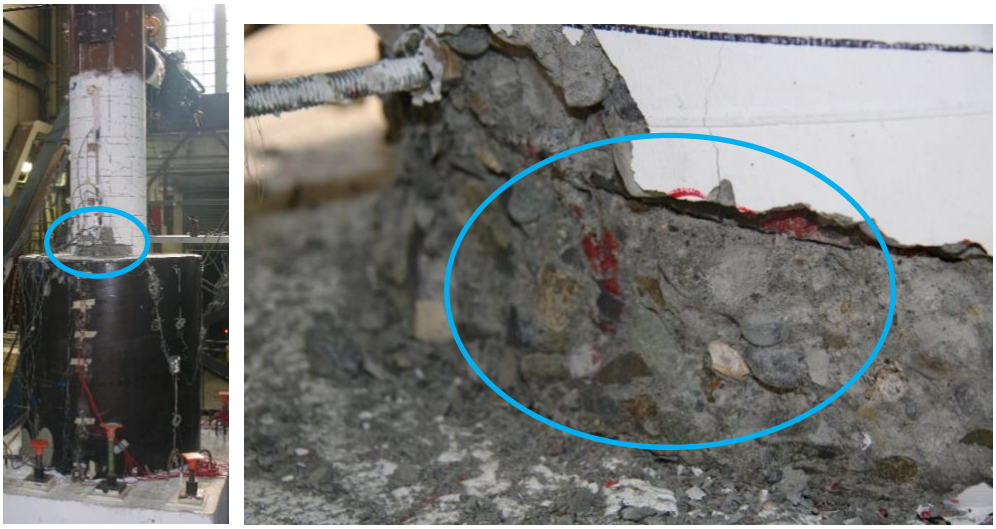

Figure 4.34. Specimen 48-21 Exposed Transverse and Longitudinal Reinforcement at 4.1% Drift

The strains measured at the peak displacement of these cycles all exceeded the yield of the reinforcement, reaching a maximum strain of 0.036 in/in at -0.15D_{COL} on the S bar, shown in Figure 4.35. The -0.75D_{COL} location did not reach the yield strain, with a max strain of .0020 in/in.

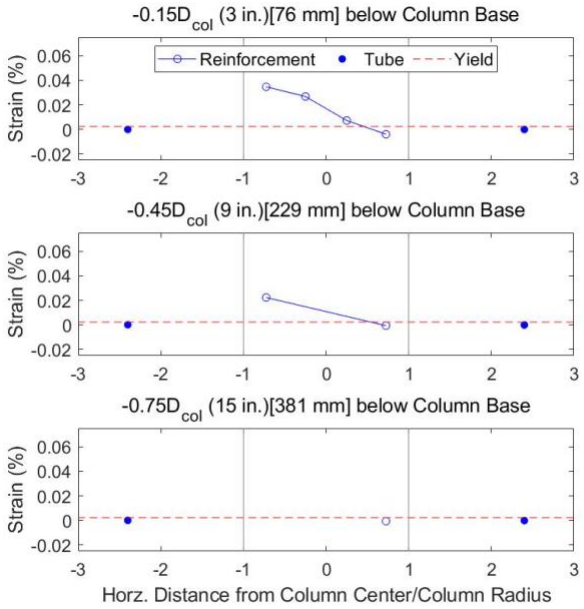

Figure 4.35. Specimen 48-21 Strain Distribution at 4.1% Drift

At drift cycles of 5.8%, the lateral load ranged from -1.4 to $1.4F_n$ (-84.7 to 84.8 kips), approximately equivalent to the last cycle. The lateral load of $1.4F_n$ (84.8 kips) was the largest lateral load the column experienced during this test. During this cycle, the column experienced its largest moment, $1.4M_n$ or 436.5 kip-ft.

The concrete on the inside of the column transverse reinforcement spalled, which completely exposed the transverse reinforcement. Spalling on the north face increased to a point where longitudinal reinforcement bars, the two bars on the northern face, were exposed. The largest measured crack was again at the base of the column on the southern face and had increased in width to 5 mm. During the second cycle, the Northern column longitudinal reinforcement bar buckled approximately 5 in. from the base of the column as shown in Figure 4.35. While the picture makes it seem like the bar is not buckling, slight buckling was observed as the column was being pushed to the left in the photo, but the bar was still bent to the right.

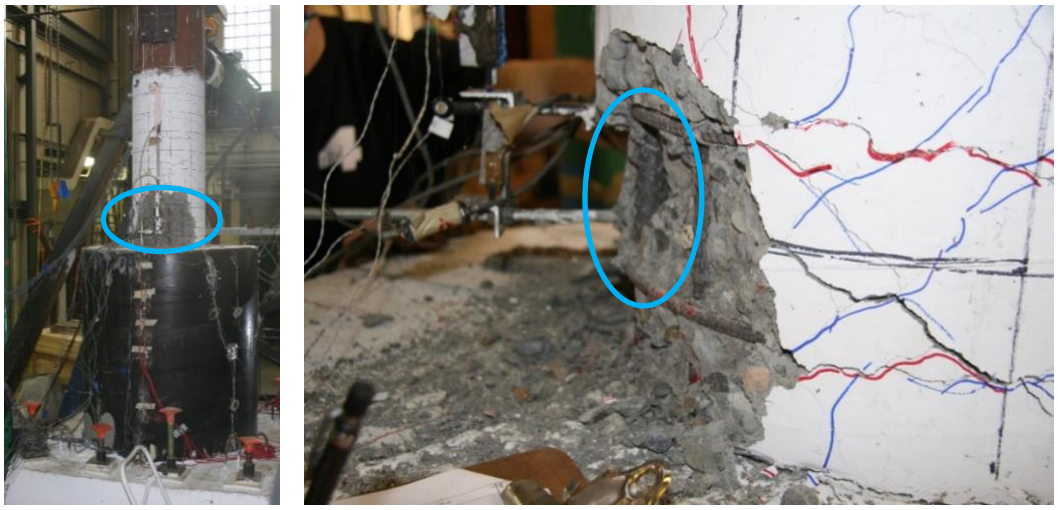

Figure 4.36. Specimen 48-21 Buckled Longitudinal Reinforcement at 5.8% Drift

At 8.6% drift, the largest lateral load was $0.6F_n$ (37.1 kips) a decrease of $0.8F_n$ (48 kips) from the previous cycle, which was also the peak force.

There was significant concrete crushing and the longitudinal bars buckled in both compression and tension, this is shown in Figure 4.37. The spalling was so widespread that horizontal cracks could not be measured.

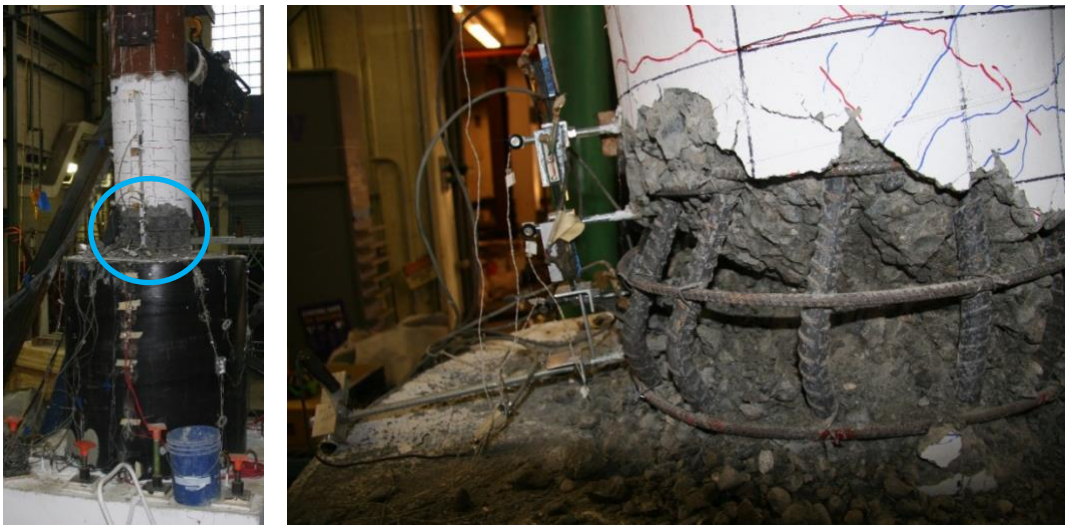

Figure 4.17. Specimen 48-21 North Face Severely Buckled Longitudinal Reinforcement Bars at 8.6% Drift

Loading was terminated after 9.7% drift, with all bars buckled and the concrete at the base of the column had completely crushed. The bottom $0.15D_{COL}$ (3 in.) of the column concrete separated from the rest of the pile. This cycle had a peak lateral load of $0.5F_n$ (32.8 kips) in compression and $0.2F_n$ (12.7 kips) in tension, resulting in a force loss of 41 kips from the previous cycles at 6% drift or 70% loss in strength from the peak lateral load of 84.8 kips. Similar to Specimen 30-21, during both of these final two cycles, the concrete at the base of the column seemed to explode out, as did the transverse reinforcement at the base too. The final state of the specimen can be shown in Figure 4.38.

Figure 4.38. Final State of Specimen 48-21 after 9.7% drift

Throughout all load cycles, the pile and transfer block showed no visible damage. There was no buckling or yielding of the pile, with the largest measured strain being 0.00017 in/in, which occurred at 52 in. below the top of the tube, during the 4.1% drift cycles. No cracks formed anywhere on the transfer block. A 3 in. section of the transfer block did break off when moving the specimen onto the testing rig and was not related to the actual testing of the specimen. There was no noticeable slip between the pile concrete in comparison to the edge of the tube at any point of the test. As shown in Figure 4.39, except for the radial cracks, the top of the pile concrete appears largely undamaged.

Figure 4.39. Top of Specimen 48-21 Pile with Column Removed

Due to using the new axial bearing rig described in Chapter 3, there was no significant binding at the top of the column. The top of the column did shift to the East during the test due to the base of the column deforming, but any touching of the top of the column CFST and the guiding channel did not have noticeable effects during the test.

Chapter 5. SUMMARY AND CONCLUSIONS

The experimental research program was conducted to investigate the connection between a RC column and a CFST pile and the effects of various parameters. The following sections contain a summary of the tests performed and observed behavior, conclusions from the tests, and suggest future topics for similar research to explore.

5.1 SUMMARY OF RESEARCH

CFSTs have been shown to be excellent composite structural components as columns and as piles for bridges due to both their strength and ductility characteristics and their cost-effectiveness. One of the most common uses of CFST components in bridge construction is for deep piles. This research provided an initial experimental investigation into the seismic performance of a direct RC pier column to a CFST pile or drilled shaft for accelerated construction of high speed rail or other transportation systems.

Two half-scale specimens were tested under cyclic loading. For these specimens, the longitudinal reinforcement of the RC pier column was embedded the full development length according to AASHTO (21 inches). A 20 in. RC pier column was employed for both specimens, but CFST pile had a 30 in. diameter pile for one specimen and a 48 in. diameter piles for the other specimen. The specimens were tested at the University of Washington in an existing test rig. The RC pile column stub was directly connected to the CFST pile. The CFST piles were embedded into a RC transfer block for anchorage into the test rig. The concrete used for the RC pier and CFST pile fill had the same design strength of 4000 psi. The reinforcing was specified as A706 Gr. 60. The 30 in. diameter tube had a grade of API 5L X52 and the 48 in. diameter tube had a grade of API 5L X42.

The specimens were tested under combined axial and lateral loading of the column. The axial load was applied using a 2400 kip Universal Testing Machine and the lateral loads were applied using a 200 kip MTS actuator attached to a self-reacting test frame. The axial load was approximately 7.5% of the gross axial capacity of the column based on measured strength.

While testing, the following observations were made:

- Yielding of the column reinforcement occurred during smaller cycles at approximately 0.6% column drift
- Spalling that exposed the column transverse reinforcement occurred during moderate cycles between 3.7% to 5.5% column drift
- Spalling that exposed the column longitudinal reinforcement occurred during moderate cycles between 4.1% to 5.5% column drift
- Extensive buckling of the column reinforcement occurred during larger cycles ranging 7.5% to 8.8% drift for all specimens not tested under long duration loading
- All tests were terminated due to lateral strength resistance loss caused by bar buckling and concrete crushing during large drift cycles between 8.1% to 9.9% column drift
- Specimens 30-21 experienced more damage, radial cracks, and concrete spalling, to the top of pile concrete than the other two specimens. Specimen 48-21 had limited radial cracks on the top of the pile concrete.
- The pile and transfer block showed no visible or measured damage for either test.

5.2 Research Results and Conclusions

- Composite action between the column and the CFST pile occurs at approximately 15 in. below the column base

- The 48 in. pile connection showed better overall performance than a 30 in. pile connection, both in terms of strength degradation, deformation capacity, specimen damage, and slip between the steel tube and the connection concrete. However, it is not possible to investigate the internal damage in these specimens.
- Using CFST piles, in a direct column to pile connection, can reduce project costs and enable accelerated construction through the reduction of labor and materials due to the elimination of formwork and internal reinforcement inside the pile

BIBLIOGRAPHY

[1] American Association of State Highway and Transportation Officials. (2017). *AASHTO LRFD Bridge Design Specifications*. American Association of State Highway and Transportation Officials (AASHTO), Washington, DC.

[2] American Association of State Highway and Transportation Officials. (2015*). Guide Specifications for LRFD Seismic Bridge Design with 2012, 2014 and 2015 Interim Revisions*. American Association of State Highway and Transportation Officials (AASHTO), Washington, DC.

[3] American Concrete Institute. (2014). *Building Code Requirements for Structural Concrete (ACI 318-14)*. Farmington Hills, MI.

[4] California Department of Transportation (Caltrans). (2019). *Seismic Design Criteria*. Sacramento, CA

[5] Chang, M. (2021). *Seismic Performance of Column-to-Drilled-Shaft Connections in RC Bridges,* Thesis, University of Washington.

[6] Kappes, L., Berry, M., and Stephens, J. (2013). *Performance of Steel Pipe Pile-to-Concrete Cap Connections Subjected to Seismic or High Transverse Loading,* Technical Report FHWA/MT-13-001/8203, Montana Department of Transportation.

[7] Kortum, Z. (2021). *Impacts of Cascadia Subduction Zone M9 Earthquakes on Bridges in Washington State: SDOF Idealized Bridges,* Thesis, University of Washington.

[8] Liu, Y. (2012). *Lateral Behavior of RC Columns Supported on Type II Shafts*, M.S., University of California, San Diego.

[9] Mehraein, M. (2016). *Seismic Performance of Bridge Column-Pile-Shaft Pin Connections for Application in Accelerated Bridge Construction,* Dissertation, University of Nevada, Reno.

[10] Stephens, M. T. (2016). *Design Expressions and Dynamic Evaluation of CFST Bridges Subjected to Seismic Hazards,* Dissertation, University of Washington.

[11] Tran, H. V. (2015). *Drilled Shaft Socket Connections for Precast Columns in Seismic Regions,* Dissertation, University of Washington.

[12] Washington State Department of Transportation (WSDOT). (2020). *Bridge Design Manual (LRFD) M 23-50*. Olympia, WA.

[13] Yeutter, A. S. (2020). *A RC Slab to CFT Column Connection for Improved Seismic Behavior of Multi-Story Buildings,* Thesis, University of Washington.

APPENDIX 1 –SPECIMEN DRAWINGS

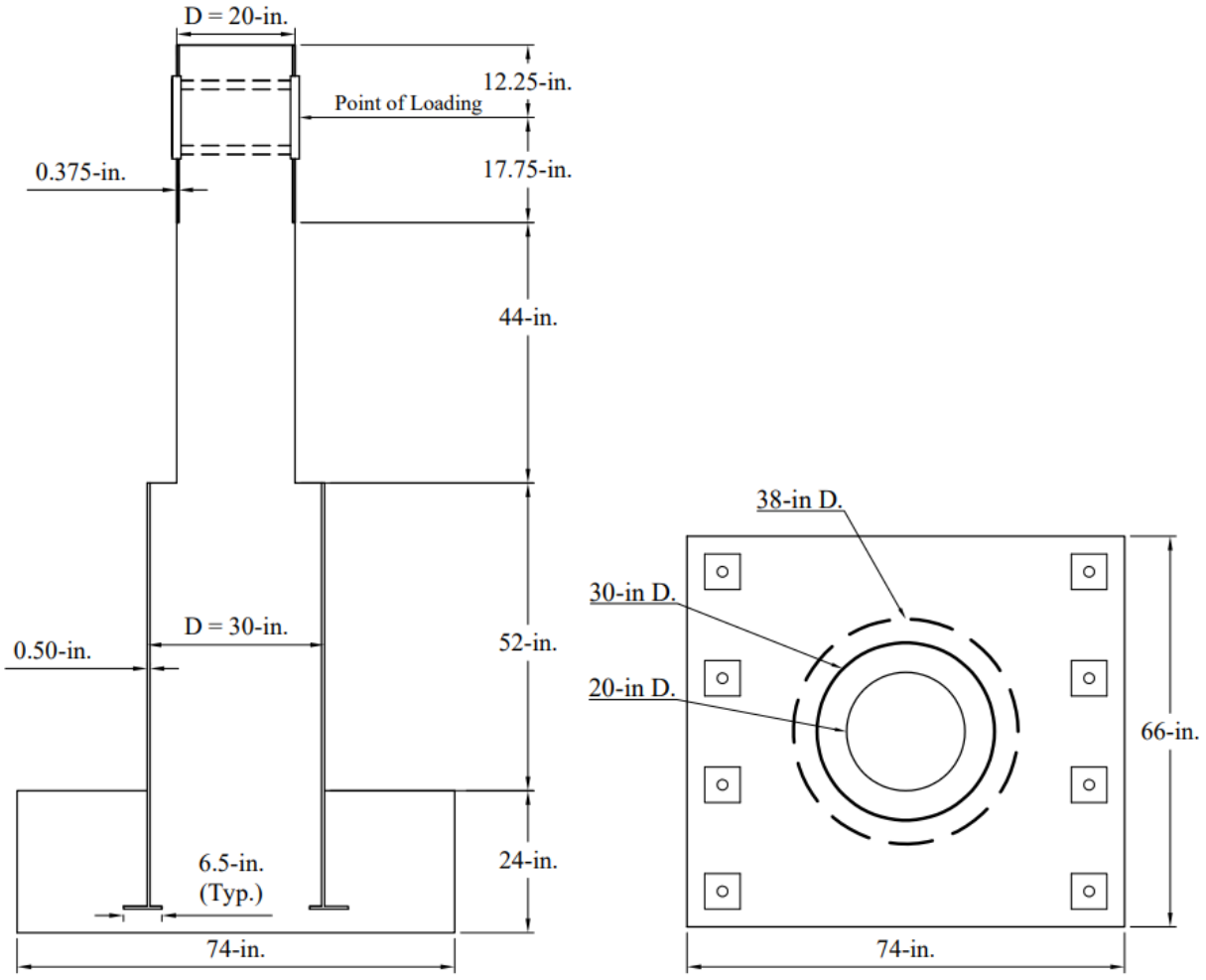

Figure A1.1 Specimen 30-21 and 30-21-LD Dimensions

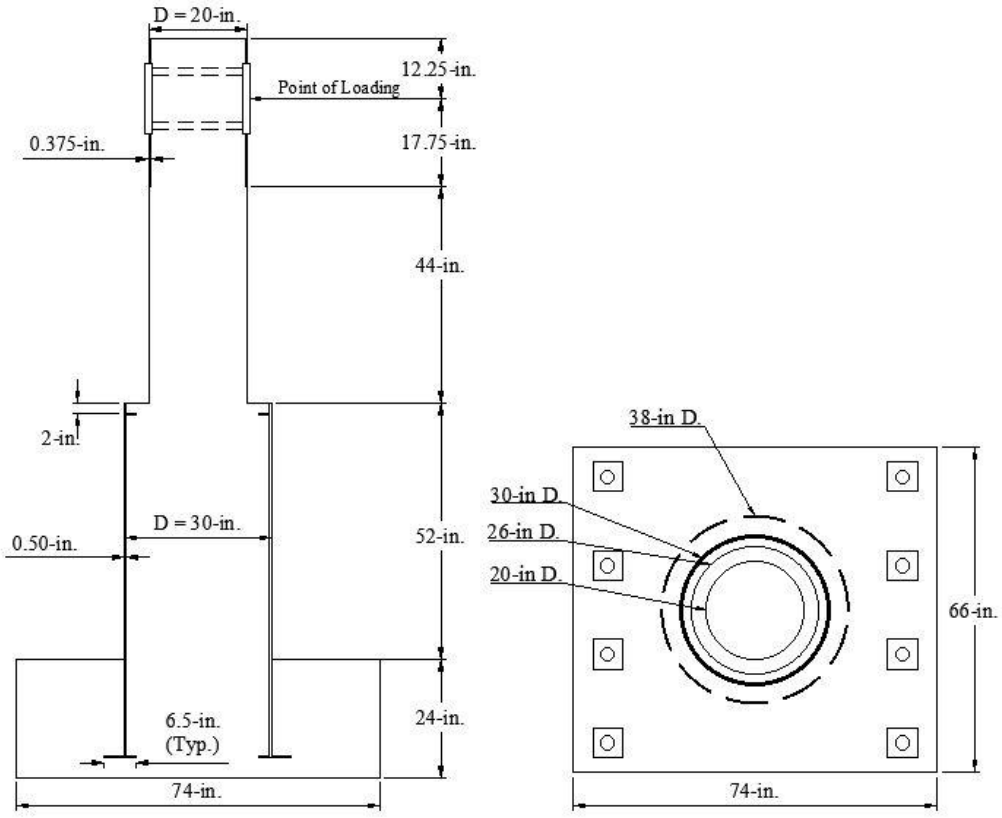

Figure A1.2 Specimen 30-21-R Dimensions

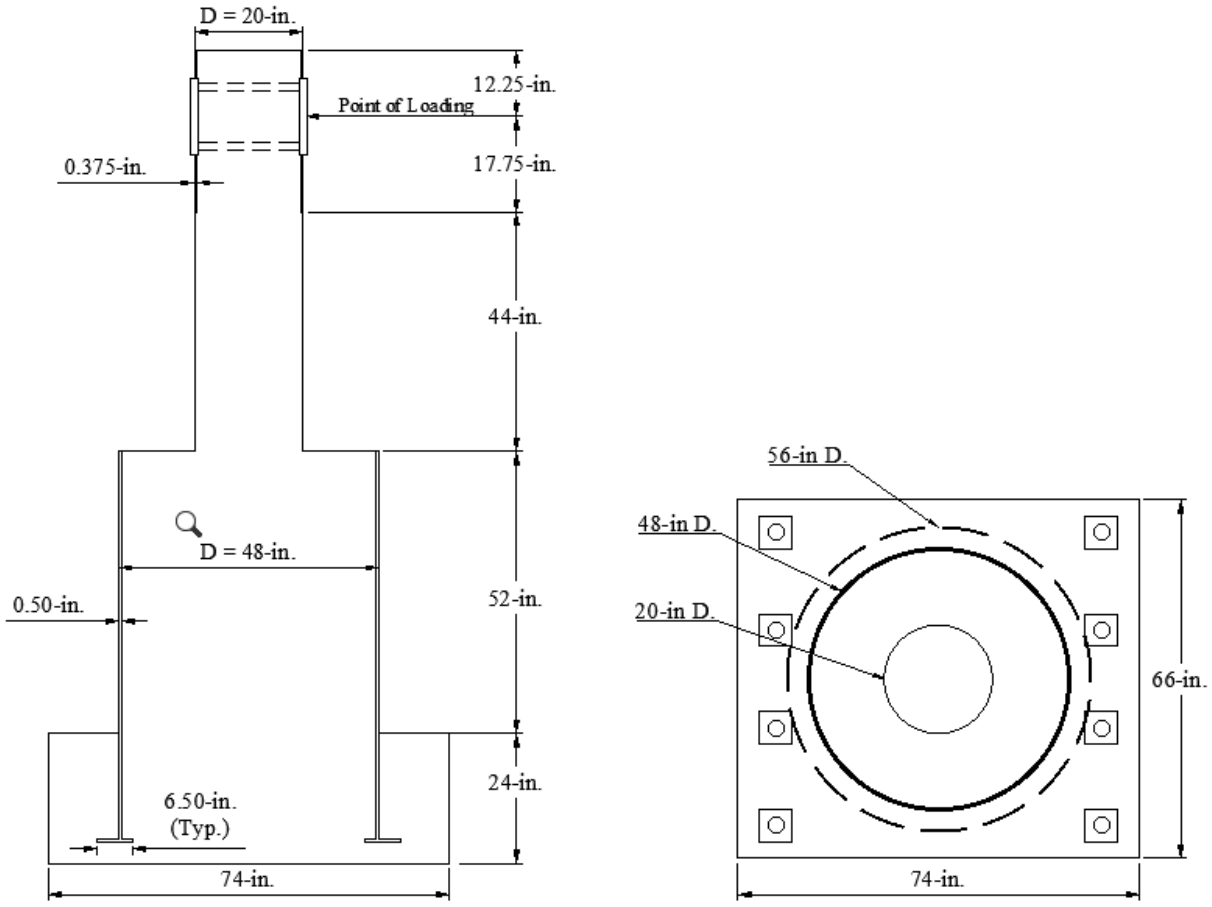

Figure A1.3 Specimen 48-21 Dimensions

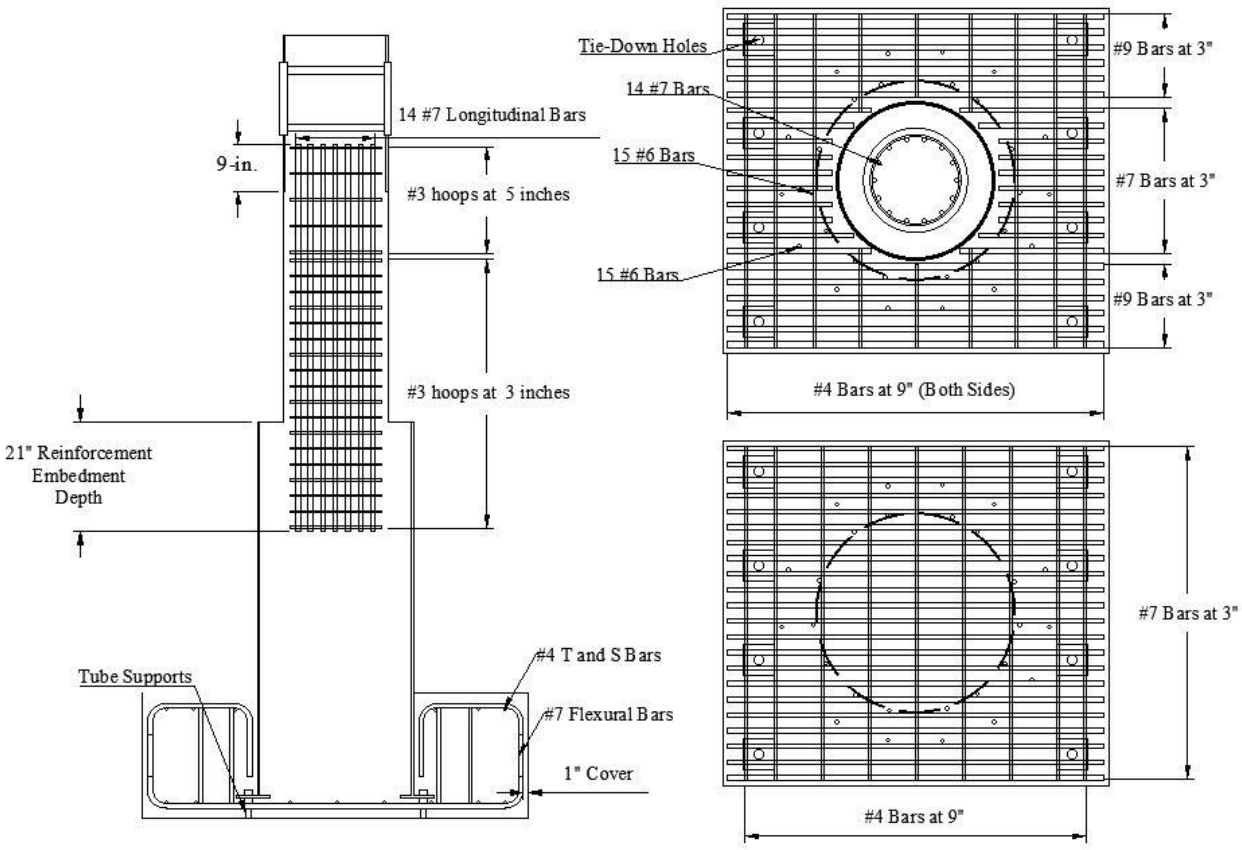

Figure A1.4 Specimen 30-21 Reinforcement Layout

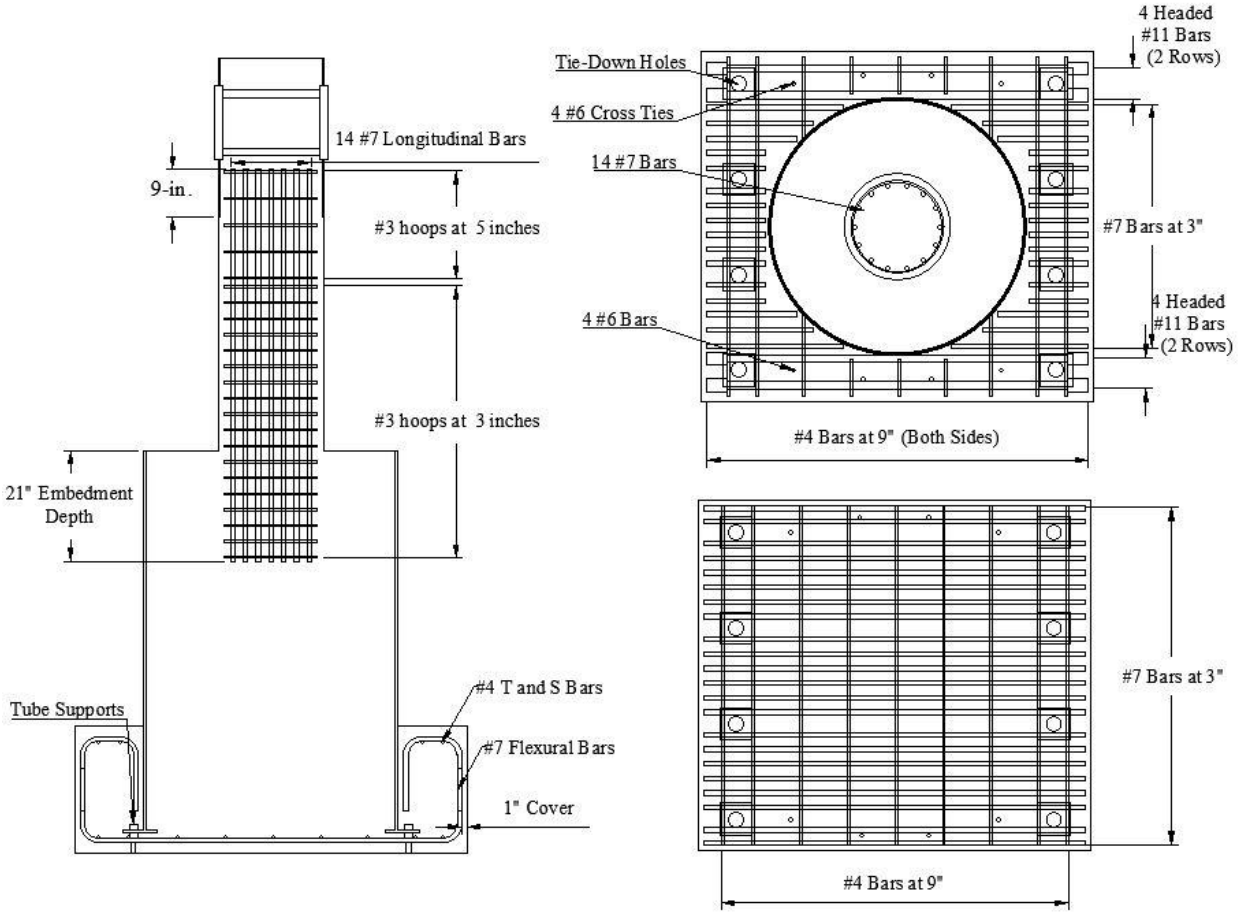

Figure A1.6 Specimen 48-21 Reinforcement Layout